CHARACTERIZATION OF MATERIAL AND COMPOSITIONAL PROPERTIES OF ILIAC BONE FROM POSTMENOPAUSAL WOMEN WITH WORSENING GLYCEMIC CONTROL

A Thesis

Presented to the Faculty of the Graduate School

of Cornell University

In Partial Fulfillment of the Requirements for the Degree of

Master of Science

by

Sashank Lekkala

August 2020

ABSTRACT

Individuals with type 2 diabetes mellitus (T2DM) have a greater risk of bone fracture compared to those with normal glucose tolerance (NGT) despite normal to high bone mineral density even after accounting for confounders like falls, BMI, and comorbidities. In contrast, individuals with impaired glucose tolerance (IGT) have a lower or similar risk of fracture.

Our objective was to understand how progressive glycemic derangement affects the composition and mechanical properties of iliac bone from postmenopausal women with NGT (n = 35, age = 65±7y, HbA1c = 5.8%±0.3%), IGT; n = 26, age = 64±5y, HbA1c = 6.0±0.4%), and overt T2DM on insulin (n = 23, age = 64±6y, HbA1c = 9.1%±2.2%). The samples from NGT and T2DM were imaged with confocal/second harmonic generation microscopy to spatially resolve fluorescent advanced glycation endproducts (fAGEs) and collagen alignment. A subset of samples (n = 14 NGT, n = 14 T2DM) with the lowest serum bone resorption marker, CTx was analyzed with nanoindentation and Raman microscopy.

Cortical bone from the T2DM group was stiffer (+9%, $p = 0.021$) and harder (+8%, $p = 0.039$) compared to that from the NGT group, but the trabecular bone had similar material properties across groups. Fluorescent AGE content was greater in bone from the T2DM vs. the NGT group (cortical +77%, $p < 0.001$; trabecular +57%, $p < 0.001$) and modestly correlated with HbA1c ($R2 = 0.33$, $p < 0.001$), but Raman spectroscopic properties did not differ across groups. When tissue material properties were assessed by sub-region (Cortical: osteonal, interstitial; Trabecular: fluorochrome label, center, edge), the relatively older tissue had higher stiffness, hardness, fAGE content, mineral content and crystallinity, and collagen maturity compared to the younger tissue. These results demonstrate that bone tissue fAGEs, which have previously been

shown to embrittle bone, increase with worsening glycemic control. This relationship suggests a potential mechanism by which bone fragility may increase despite greater tissue stiffness and hardness in individuals with T2DM.

BIOGRAPHICAL SKETCH

Sashank Lekkala graduated with a bachelor's degree in Mechanical Engineering from the Indian Institute of Technology, Varanasi, in 2018. In his junior and senior years, he worked in the lab of Dr. Marshal Dhayal, where he developed a profound interest in the field of biomaterials. Dr. Marshal encouraged Sashank to continue his education, and Sashank decided to pursue an MS in Materials Science and Engineering at Cornell University. At Cornell, Sashank worked with Dr. Eve Donnelly studying the effects of type 2 diabetes on bone material and compositional properties. Upon graduation, Sashank will work with Dr. Ebru Oral at Harris Orthopedics Lab in Massachusetts General Hospital where he will work on developing novel, therapeutic total joint implants.

ACKNOWLEDGMENTS

Firstly, I would like to extend my sincere gratitude to my advisor, Dr. Eve Donnelly for her unwavering support and belief in my abilities throughout the project. She consistently guided me to develop skills to become a responsible and a disciplined researcher. I am extremely grateful to Dr. Donnelly for all the helpful advice and for being an incredible role model.

I would also like to thank Dr. Shefford Baker for providing access to the nanoindenter in his lab, and his graduate student, Zach Rouse for training and help with the instrument. I would also like to acknowledge Dr. Rebecca Williams and Johanna Dela Cruz for assistance with multiphoton imaging. This research would not have been possible without our collaborator Dr. Kendall Moseley at Johns Hopkins Medicine.

TABLE OF CONTENTS

CHAPTER 1

EFFECTS OF DIABETES ON BONE MATERIAL PROPERTIES

1.1 Introduction

Individuals with type 1 and type 2 diabetes mellitus (T1DM, T2DM) share a common complication of greater fracture risk relative to controls without DM [1,2]. In meta analyses, the risk of hip fracture is greater in individuals with T1DM (RR = 6.9 [1], 6.3 [2]) and in individuals with T2DM (RR = 1.4 [1], 1.7 [2]), both compared to controls without DM. Bone mineral density (BMD) is lower in individuals with T1DM compared with an age-matched control population [1]; however, the increased fracture risk in T1DM is not explained by the decreased BMD in this population [3]. On the other hand, individuals with T2DM have normal or even greater BMD compared to an age-matched control population [1], yet the increased fracture risk with T2DM persists after adjustment for BMD and potential confounders like BMI and falls [4,5]. Despite the increased risk of falls in individuals with DM due to several risk factors [6], falls do not completely account for the increased fracture risk [3,7]. Therefore, metabolic or biochemical changes associated with DM may alter aspects of the bone microstructure and tissue properties independently of the bone mass, though the precise mechanisms responsible for these changes may be T1DM- or T2DM-specific.

The mechanisms by which diabetes mellitus may degrade the fracture resistance of bone are complex, as addressed in several recent reviews [3,8–10]. In T1DM, pancreatic beta cell failure and insulin/IGF1 deficiency impair osteoblastic bone formation and inhibit accrual of peak bone mass during growth, and advanced glycation endproducts (AGEs) may directly and indirectly alter matrix properties [8,9]. In T2DM, a constellation of factors comprising

hyperglycemia; oxidative stress; fat-derived inflammatory cytokines and adipokines; and AGEs collectively inhibit osteocyte function, alter bone turnover, and degrade collagen properties [9]. Facets of bone quality that may contribute to decreased fracture resistance in diabetic bone include altered bone microarchitecture and tissue material properties, which may arise from disease-induced changes in bone formation or remodeling, as well as direct alteration of collagen matrix properties by accumulation of AGEs. AGEs are the reaction products of reducing sugars with free amino groups in proteins and result in a diverse array of structures including crosslinking and non-crosslinking products. Crosslinking AGEs have been implicated in embrittling bone tissue in men with T2DM [11], rodent models of T2DM [12], and in *in vitro* ribosylation/glycosylation studies [13,14]. Non-crosslinking AGEs, like carboxymethyl lysine (CML), can also be deleterious to bone tissue through interactions with the receptor for AGEs (RAGE), which induces oxidative stress and inflammation [15].

The objective of this review is to summarize work that elucidates the material factors that may contribute to fragility in T1DM and T2DM. Many studies have evaluated alterations in BMD and bone microarchitecture in patients with DM (reviewed in [1,2,16,17]); here we focus on investigations that have evaluated the changes in tissue-level compositional and mechanical properties associated with diabetic bone disease.

1.2 Type 1 Diabetes Mellitus

In individuals with T1DM, insulin/IGF1 deficiency impairs osteoblastic bone formation and inhibits accrual of peak bone mass during growth, resulting in characteristically low bone formation rates and low BMD [1,8]. Decreased osteoblast activity and survival have generally been observed in both humans and animals with T1DM; however, the activity of osteoclasts is not yet well characterized, with the limited studies available reporting either no changes or

increases in bone resorption [18]. Low turnover in patients with T1DM is evident in several markers (recently reviewed in [19]): lower osteocalcin, a bone formation marker; lower C-terminal telopeptide (CTx), a bone resorption marker; and higher sclerostin, a potent inhibitor of the Wnt signaling pathway. Further, hyperglycemia; hypoinsulinemia; autoimmune inflammation; and low levels of insulin-like growth factor-1 (IGF-1), osteocalcin, and vitamin D observed in patients with T1DM may additionally contribute to bone fragility [20,21]. Finally, accumulation of AGEs may embrittle the matrix or alter bone turnover [13,14]. These mechanisms are yet to be confirmed by studies on human patients with T1DM.

1.2.1 Human Studies

Trabecular bone from patients with T1DM and history of a prior fragility fracture had greater mineral content and concentrations of AGEs than age- and sex-matched controls [22]. Specifically, in a case-control study of iliac crest biopsies (n = 5/group), the concentration of the AGE, pentosidine (Pen) measured by HPLC and degree of mineralization measured by microradiography was higher in trabecular bone in patients with T1DM with a prior fracture vs. that of non-diabetic non-fracture controls [22]. However, no significant changes in Pen and degree of mineralization were observed between patients with T1DM without a history of fracture and non-diabetic non-fracture controls. Serum HbA1c was positively correlated with trabecular Pen, suggesting that AGE accumulation increases with worsening glycemic control in this cohort. Together, both high Pen content and mineralization may embrittle the bone matrix and contribute to the bone fragility observed in patients with T1DM. A key limitation of this study is that patients with any complications of DM—who are at a greater relative risk for fracture than those without complications [1]—were excluded from the study, which may have attenuated potential differences between T1DM and control groups. Studies of a larger cohort

and greater range of disease severity are required to confirm these observations in a broad T1DM population.

The mechanical behavior of bone from patients with T1DM has been characterized in a small number of opportunistic studies, which have generally noted modest effects of T1DM. Cortical and trabecular bone at the iliac crest from patients with T1DM trended toward being stiffer and harder vs. non-diabetic controls at the nanoscale as assessed by nanoindentation, but were not different at the microscale as assessed by Vickers microindentation [22]. Ultimate stress and Young's modulus estimated by whole-bone three-point bending did not differ in patients with T1DM undergoing amputation of the 2^{nd} - 5^{th} metatarsal (mean age = 51 years) vs. aged controls from deceased donors (mean age = 72 years) [23]. Similarly, estimated elastic modulus, yield strength, and ultimate strength assessed by three-point bending of tibial explants did not differ in patients with T1DM (mean age = 51 years) vs. aged controls (mean age = 75 years) [24]. A limitation of these studies is that the microarchitecture, which may potentially reflect altered gait and vasculature in patients with T2DM, was not characterized; therefore, the outcomes of three-point bending were not adjusted for potential differences in bone volume fraction (BV/TV). These results suggest that changes in mechanical properties of human bone with T1DM may be similar to those of aging in a non-diabetic environment; however, this assertion awaits confirmation in future studies with age-matched controls across multiple anatomic sites.

Assessment of bone material properties at the tissue level in clinical samples of patients with T1DM is limited. Thus, an urgent need in the field is to confirm changes in tissue-level composition and mechanical properties observed in animal models of T1DM (see below) with studies in humans to improve our understanding of the mechanisms of clinical fracture in T1DM

populations.

1.2.2 Animal Models

Studies of the effects of T1DM on bone material properties have predominantly been conducted in animal models and have demonstrated changes in mineral and collagen properties and mechanical behavior.

Streptozotocin-Induced Diabetes

T1DM can be induced in mice and rats with streptozotocin (STZ) injections, typically at 8-12 weeks of age, which causes necrosis of pancreatic beta cells thereby inducing permanent diabetic hyperglycemia. STZ-induced T1DM rodents present similar blood glucose (>300 mg/dl) and plasma insulin levels as T1DM syndrome in humans [25]. However, the effects of STZ vary in rats and mice (Table 1.1). This difference may be partly attributed to differences in timing of induction of T1DM relative to lifespan. Induction of T1DM at 8-10 weeks occurs before skeletal maturity in rats (15 to 17 weeks [26]), potentially causing more profound deficits in composition and mass accrual of bone, but near skeletal maturity in mice (10 to 12 weeks [26]), potentially modeling the effects of later onset of T1DM. Overall, bone tissue of STZ-induced T1DM rats showed decreased collagen maturity—assessed by the ratio of mature trivalent to immature divalent enzymatic crosslinks [27] —and increased AGE accumulation vs. vehicle-injected controls [28–32], whereas T1DM mice showed increased collagen maturity vs. vehicle-injected controls [33].

STZ injections may also have differential effects on mineralization and mineral properties in rats compared to mice. In rats, STZ injection decreased the mineral:matrix ratio, the ratio of mineral content to organic matrix content, assessed by FTIR imaging in femoral cortical and trabecular bone [29] but increased humeral ash content [31] vs. controls. In contrast, in mice,

STZ injection did not alter the FTIR mineral:matrix ratio [33] or calcium content assessed with quantitative backscattered electron imaging (qBEI) [32] vs. controls. C-axis mineral crystal length observed by x-ray diffraction [34] was shorter consistent with higher carbonate:phosphate [29] in STZ-injected rats vs. controls. The variable reports on changes in mineral properties with STZ-induced T1DM may arise from the use of different measurement techniques and different outcomes across studies, e.g., multiple mineral:matrix ratios [35,36]. Nevertheless, the STZ-injected rat model currently best reflects the changes in material properties observed in humans with T1DM (Table 1.1).

In STZ-induced T1DM, at the tissue level, lower nano- and microhardness were observed; while at the whole-bone level, the bones were had reduced strength and toughness in bending [30,31,34,37,38]. Reduced nanoindentation modulus, hardness and Vickers microhardness were observed in the femoral cortex of STZ-injected mice vs. vehicle-injected controls [37].

Combined, the impaired tissue-level and whole-bone mechanical properties with STZ-induced T1DM contributes to our understanding of the effects of T1DM on bone biomechanical performance and may partially explain the increased fracture risk with T1DM. Further studies are needed to quantitatively relate tissue-level compositional changes with mechanical properties at multiple levels of structural hierarchy.

OVE 26 Mouse Model

The OVE 26 mouse model demonstrates systemic changes of severe and progressive T1DM through overexpression of calmodulin, which regulates insulin secretion by pancreatic B-cells [39,40]. This model shows similar changes in collagen properties to STZ-injected mice. Enzymatic and non-enzymatic collagen crosslinking are increased in OVE 26 mouse femurs vs.

wild type (WT) controls. Specifically, pyridinoline content measured by Raman spectroscopy, an outcome similar to collagen maturity measured by FTIR spectroscopy, was increased in OVE 26 mice vs. WT controls [39]. Additionally, the AGEs CML and Pen, measured by Raman spectroscopy, were increased in OVE 26 mice vs. WT controls [39]. The increase in AGE content, which may arise from increased serum glucose levels with T1DM, is associated with decreased remodeling and osteoclast activity and may explain the increase in enzymatic crosslinking. However, alterations in the mineral phase of OVE 26 mice suggest biological activity different from those that drove the observed change in the collagen phase. The Raman mineral:matrix ratio of bone tissue in OVE 26 mice was reduced vs. WT controls [39], which suggests impaired bone formation/osteoblast activity or increased remodeling/osteoclast activity.

In addition, tissue-level resistance to crack initiation and propagation is impaired in the OVE 26 mouse. Initiation toughness and propagation toughness, measured by whole-bone notched bending, were decreased, and indentation distance increase (IDI, difference in indentation distance into the bone between first and last cycles), measured by cyclic reference point indentation (RPI), was increased in OVE 26 mice vs. WT controls [39]. Furthermore, inverse correlations were observed between CML and Pen with initiation toughness and propagation toughness in both OVE 26 and WT mice [39]. Combined, the greater collagen crosslinking and reduced mineral content observed in the OVE 26 mouse may explain the observed decrease in resistance to fracture of the femur compared to non-diabetic controls.

Table 1.1. A symbolic summary of the effects of T1DM on bone material properties in humans and polygenic rodent models. Each arrow represents the result of one study with compositional, material, or structural outcomes indicated as increased (↑), decreased (↓), and unchanged (↔) vs. non-diabetic controls. Material properties reported here were both directly assessed and estimated from whole-bone tests. Abbreviations: XST = mineral crystallinity; C:P = Carbonate:Phosphate ; XLR = collagen maturity; Pen = Pentosidine concentration; E = elastic modulus; σ_y = yield stress; σ_{ult} = ultimate stress; K= fracture toughness; P_{max} = maximum load; IDI = Indentation distance increase.

	Mineral composition			**Collagen composition**				**Material properties**						**Structural properties**	
	Mineral content	XST	C:P	XLR	Enzymatic Crosslinks	Pen	fAGEs	E	σ_y	σ_{ult}	Toughness	K	IDI	P_{max}	Stiffness
Humans [22]	↑					↑									
STZ rats [28–31,34,38]	↓↓/↔/↑	↓/↔	↓/↔	↓↓↓	↑/↔	↑		↓↓/↔ ↔↔	↓/↔	↓↓↓/ ↔↔	↓↓/↔			↓↓↓	↓↓/↔
STZ mice [32,33,37]	↔	↔	↔	↑↑				↔	↔	↔	↓/↔			↓	↓
OVE 26 mice [39]	↓	↔			↑	↑						↓	↑		

1.3 Type 2 Diabetes Mellitus

In contrast to T1DM, which is characterized by a lack of insulin production, T2DM develops in response to insulin resistance. T2DM is characterized by hyperglycemia and hyperinsulinemia, which may differentially alter bone material properties. Hyperglycemia disrupts bone remodeling via osteoblasts and osteoclasts. In addition, excess glucose can alter bone tissue material properties through the accumulation of AGEs and downstream effects of AGE-RAGE interactions. On the other hand, insulin is an anabolic agent, and hyperinsulinemia may help explain the greater BMD observed in people with T2DM [41]. Moreover, insulin signaling helps regulate osteoblastic proliferation and supports osteoclastogenesis [42]. The extent to which bone remodeling and material properties are affected by the simultaneous effects of hyperglycemia, AGE accumulation, and hyperinsulinemia, is not yet known.

Several recent studies of clinical specimens have given insight into the properties of human tissues from patients with T2DM. Additionally, in vitro glycation studies provide a basis for hypothesized changes to bone material properties in vivo. Finally, studies of bone metabolism, mass and structural properties in several animal models of T2DM, are reviewed elsewhere [26]; here we focus on the changes in material properties observed in these models.

1.3.1 Human Studies

Two recent studies related compositional changes with T2DM to mechanical properties in the proximal femur of subjects undergoing total hip arthroplasty. In the first study, cortical tissue from the T2DM group trended towards having greater total fluoresent AGE (fAGE) content (+21.3%, $p = 0.09$) and exhibited greater indentation distance and IDI measured by cyclic RPI of vs. the non-DM control group. However, the total fAGE content and most monotonic compression properties (with the exception of yield stress) did not differ between groups in the

cancellous tissue [43]. In the second study, cancellous tissue in the T2DM group had greater Pen concentration and lower pyridinoline concentration assessed by HPLC, greater sugar:matrix and mineral:matrix assessed by FTIR, no difference in total fAGE content, and greater compressive stiffness and strength normalized by bone volume fraction vs. the non-DM control group [11]. Moreover, statistical models from the latter study demonstrated that T2DM has both beneficial and adverse effects on the apparent-level mechanical behavior of cancellous bone. Patients with T2DM had numerically higher BV/TV (+24%, NS, $p = 0.13$), which had a large positive effect on bone strength, stiffness, and toughness vs. controls. In contrast, after accounting for the effects of BV/TV, bone tissue from patients with T2DM exhibited adverse effects of Pen, total fAGEs, and mineral maturity on post-yield toughness. Individuals with T2DM that have average or greater changes in tissue composition related to T2DM (e.g., AGE accumulation or mineral maturity) but do not have the protective effect of greater BV/TV are at a greater risk of bone embrittlement compared to those with or without T2DM that do not have this set of deleterious tissue changes. Individuals with T2DM that have average or greater changes in tissue composition related to T2DM (e.g., AGE accumulation or mineral maturity) but do not have the protective effect of greater BV/TV are at a greater risk of bone embrittlement compared to those with or without T2DM that do not have this conglomeration of deleterious tissue changes. Additionally, Pen content measured in tibial explants of men undergoing total knee replacement was higher in the DM group (9 patients with T2DM and 1 patient with T1DM) vs. non-diabetic controls [44]. Therefore, these studies provide evidence that T2DM is associated with accumulation of AGEs and that these compositional changes adversely affect bone tissue properties.

Additionally, alterations in mineral properties have also been observed with T2DM in similar clinical specimens. A higher mean calcium concentration and a narrower distribution of mineralization were observed in trabecular bone of the femoral neck in subjects with T2DM vs. non-diabetic controls [45]. These changes are consistent with the greater FTIR mineral:matrix observed in a similar patient population [11], and reduced bone remodeling with T2DM [46], which enables progression of secondary mineralization and results in a more mineralized tissue with a more homogeneous mineral distribution. Together, these studies indicate altered mineralization and increased AGE accumulation in T2DM, which may contribute to the inferior fracture resistance observed clinically at the whole-bone level. Furthermore, additional studies are needed to relate changes in tissue-level compositional and mechanical properties to disease severity and duration through long-term assessment of HbA1c in populations with a wide range of glycemic control.

In addition to the prior studies, which required ex vivo analysis of mechanical properties and composition, one key study measured the resistance of the tibial cortex to impact indentation [Bone Material Strength Index (BMSi)] in vivo in individuals with and without T2DM [47]. BMSi was lower in patients with T2DM vs. non-DM controls [17,47,48]; decreased with longer duration of diabetes [48]; and inversely correlated with 10-year HbA1c [47]. Because the relationship between BMSi and clinical fracture risk or other measures of fracture resistance is not yet well established [49], further assessment of fracture properties of bone in the T2DM population is required to interpret these data and inform estimation of fracture risk.

1.3.2 In vitro Glycation Models

In vitro glycation or ribosylation simulates exposure to high blood glucose in T2DM. These models, in which bone specimens are incubated in a solution containing glucose or ribose for

durations of ~7 days (equivalent to 2-3 decades of aging) [14,50,51], can be used to understand the mechanisms through which glycation affects the compositional and mechanical properties of bone.

In vitro glycation increases the AGE content of bone specimens compared to non-glycated controls [14,50,51]. Glycation increased non-enzymatic crosslinks assessed by FTIR, HPLC, and a fluorometric assay in the human femoral cortex vs. non-glycated controls [52]. Similarly, ribation of bovine metatarsi increased Pen, measured by HPLC, but did not change mineralization, measured by qBEI, vs. non-glycated controls [53]. These results indicate that in vitro glycation modifies the collagen crosslinking profile without altering mineralization. One limitation of this model is that it cannot capture the effects of metabolism and related dynamic changes in AGE accumulation due to remodeling in vivo. Because T2DM alters both bone mineral and matrix properties [11,43], the in vitro models are useful for understanding the effects of increased glycation associated with T2DM on the collagen properties in bone but cannot capture not all changes in bone tissue properties with T2DM.

AGE accumulation degrades post-yield properties and increases bone stiffness. Post-yield strain energy and damage fraction assessed by unconfined compression testing on femoral cancellous bone and post-yield strain measured by three-point bending of bovine metatarsi were reduced in the ribosylated group vs. non-glycated controls [14,53]. Stress at equilibrium and equilibrium modulus measured by stress relaxation tests on demineralized specimens from the mid-diaphysis of human tibiae were higher in glycated specimens vs. non-glycated controls, suggesting stiffening and residual stress accumulation in the matrix because of glycation [50]. Although these results inform the relationship between AGE accumulation and mechanical

properties *in vitro*, this relationship has been recently reported in human T2DM [11,44] but remains an area of active investigation.

1.3.3 Animal Models

Diet-Induced Obesity

A high fat diet (HFD) induces mild T2DM in C57BL/6 mice. Although this model does not produce overt diabetes, it enables examination of changes in bone material properties due to prediabetes and impaired glucose tolerance (Table 1.2).

HFD increases non-enzymatic crosslinking of collagen. Pen measured by Raman spectroscopy and total fAGEs were greater in cortical regions of the femur and tibia, respectively, in obese mice vs. lean controls [54,55]. HFD did not change the bone mineralization, crystallinity, and carbonate substitution at the femoral mid-diaphyseal cortex [54]. In addition, the carbonate:phosphate ratio in trabecular bone from the femoral distal epiphysis was lower in the obese group than in lean controls [54]. These results suggest that AGE accumulation in the bone matrix begins in a prediabetic state, while the mineral properties are only subtly altered during this period.

In general, HFD impairs structural and material performance in this model. Femurs of obese mice were weaker and stiffer vs. lean controls [54–56]. Fracture toughness assessed by notched whole-bone testing, as well as ultimate strength, yield strength, and Young's modulus estimated from whole-bone tests, were lower in obese mice vs. lean controls [55,57]. However, Young's modulus determined by finite element analysis of the femur was higher in obese mice vs. lean controls, and the Pen content positively correlated with Young's modulus, indicating that AGE accumulation increases bone stiffness [54]. Although the effects of HFD on the tissue

modulus varied across studies, altered bone material composition in HFD mice was associated with decreased bone fracture toughness.

Single Gene Mutation Models

Single gene models are spontaneous models that enable examination of the effects of an individual gene mutation on bone material properties. The Zucker Diabetic Fatty (ZDF) rat model, has a leptin receptor deficiency that leads to overt diabetes ~9-10 weeks of age, in males only [58]. The yellow Kuo Kondo (KK/Ay) mouse develops severe obesity and insulin resistance by eight weeks [59]. The ob/ob mouse is a model of severe obesity resulting from a spontaneous inactivating mutation in the leptin gene, whereas the db/db mouse is a model of severe T2DM resulting from an autosomal recessive mutation of the db gene [26]. The material properties of bone in single-gene mutation models are somewhat dependent on the mutation (Table 1.2).

At the whole-bone level, the femora and tibia of ZDF rats were weaker and more compliant in bending, and the L4 vertebrae were weaker and more compliant in compression, compared to lean controls [60,61]. Vickers microhardness did not differ in the tibial cortex of ZDF rats vs. lean controls [62]. ZDF rats had wider bone mineral density distributions (BMDDs) measured by qBEI in metaphyseal bone vs. controls, suggesting altered endochondral ossification compared to non-diabetic rats [63].

Likewise, ultimate bending load was lower in the tibiae of KK/Ay mice vs. C57BL/6 controls [64]. In addition, tissue from KK/Ay mice have an increased proportion of mature collagen crosslinks and mineral content. Mean FTIR collagen maturity was greater in femora of KK/Ay mice vs. black homozygous a/a controls [65]. Additionally, whole-femur mineral:matrix ratio, was greater in KK/Ay mice vs. a/a controls [65]. These results suggest decreased bone

turnover in KK-Ay mice, which is supported by decreased serum osteocalcin levels in adult KK/Ay mice [66].

Similarly, the femora of ob/ob and db/db mice were weaker in bending, and db/db mice had a lower estimated elastic modulus vs. C57BL/6 WT controls [67–69]. At the tissue level, the reduced modulus determined by nanoindentation of the femoral cortex was lower in db/db mice vs. WT controls [68].

Overall, single gene mutation models of T2DM have impaired mechanical performance at the tissue and whole-bone level. However, there are no studies to conclusively relate these changes to changes in bone composition. Studies assessing both compositional and mechanical properties are required to elucidate the mechanisms through which T2DM increases bone fragility.

Polygenic models

Polygenic animal models are spontaneous models that can mimic the complex genetic alterations and subsequent changes in bone material properties in patients with T2DM. These include Zucker Diabetic Sprague Dawley (ZDSD) rats, created by breeding heterozygous ZDF rats with diet-induced obese rats [60], which develop diabetes at an older age than ZDF rats. WBN/Kob rats are non-obese rats produced by selective inbreeding of Wistar rats and develop hyperglycemia by about 12 months of age [12]. The TallyHo mouse is an obese model of early onset T2DM developing hyperglycemia around 12 weeks of age [70]. Models for which, to our knowledge, there are no data on compositional properties but for which the structural properties have been reviewed recently [26], have been omitted in the current discussion.

Overall, polygenic models of T2DM show increased mineralization similar to human studies but collagen composition is not consistent across models (Table 1.2), indicating that increased mineralization could be a consistent trend across all patient groups of T2DM while collagen properties may depend on the pathogenesis.

ZDSD rats and TallyHo mice showed higher Raman Mineral:matrix ratio vs. CD(SD) and SWR/J [71] controls respectively [72,73]. Pen concentration, measured by HPLC, was similar between ZDSD rats and TallyHo mice vs. respective controls [73,74] but was greater in WBN/Kob rats vs. Wistar controls [12]. But, the distribution of collagen D-spacing, assessed by AFM in cortical regions of the tibia was altered in ZDSD rats vs. CD(SD) controls [72]. Additionally, mineral crystallinity assessed by Raman spectroscopy was greater in the femoral cortex [73] but did not differ at the tibial cortex [72] of ZDSD rats vs. CD(SD) controls. Anatomic site and duration of HFD (6-7 weeks vs. 2 weeks) may contribute to the discrepancy.

Polygenic models show improved or deteriorated structural performance at whole-bone level depending on the model. But, surprisingly the fracture toughness parameters were comparable to the controls in these models.

Femora of ZDSD rats and WBN/Kob were weaker in bending vs. respective controls [12,60,75,76]. The study on WBN/Kob rats showed that the ratio of Pen to total enzymatic crosslinks was significantly associated with all the measured mechanical properties[12]. These results suggest that load-bearing properties of bone depend on both enzymatic and non-enzymatic crosslinks. Crack initiation toughness and propagation toughness measured by notched whole-bone bending did not vary with age for CD(SD) rats but decreased with duration of diabetes in the ZDSD rats [73]. Aditionally, in cortical bone from ZDSD rats creep indentation distance assessed by RPI was lower [72]; and indentation distance increase was

lower [72] and higher [75] vs. CD(SD) controls, a difference potentially attributable to the differing indentation forces (5 N vs. 10 N) used. The altered material properties in tissue from ZDSD rats could be attributable to the increased tissue mineralization [72,73].

Structural properties measured by three-point bending of the femur were comparable to superior in TallyHo mice vs. SWR/J controls, consistent with increased cortical thickness [74,77] and greater tissue mineral content [74]. In addition, two differences in tissue-level mechanical properties have been noted : (1) lower post-yield displacement in TallyHo, indicating reduced ductility, consistent with greater mineralization [74,77] yet (2) first-cycle and total indentation distance from RPI were greater in TallyHo tibiae vs. SWR/J controls, suggesting less tissue-level resistance to indentation. Further studies assessing the outcomes of reference point indentation at different loads and anatomical regions are required to understand the significance of this result.

In summary, polygenic models show increased mineralization, altered collagen crosslinking and inferior-to-superior structural properties, and a subset show deterioration of intrinsic resistance to fracture with duration of disease (Table 1.2).

Table 1.2. A symbolic summary of the effects of T2DM on bone material properties in humans and rodent models. Each arrow represents the result of one study with compositional, material, or structural outcomes indicated as increased (↑), decreased (↓), and unchanged (↔) vs. non-diabetic controls. Material properties reported here were both directly assessed and estimated from whole-bone tests. Abbreviations: XST = mineral crystallinity; C:P = Carbonate:Phosphate ; XLR = collagen maturity; Pen = Pentosidine concentration; E = elastic modulus; σ_y = yield stress; σ_{ult} = ultimate stress; K= fracture toughness; P_{max} = maximum load.

	Mineral composition			**Collagen composition**				**Material properties**					**Structural properties**	
	Mineral content	XST	C:P	XLR	Enzymatic Crosslinks	fAGEs	Pen	E	σ_y	σ_{ult}	Toughness	K	P_{max}	Stiffness
Human [11,43–45]	↑↑	↔	↔	↔	↓/↔↔	↑/↔↔	↑↑	↑/↔	↓/↑	↑/↔	↔↔			
Obese C57BL/6 mice [54–57]	↔	↔	↓/ ↔			↑	↑	↓/↑	↓↓/↔	↓↓		↓↓/ ↔	↓↓/↔	↓↓↓

ZDF rats [60,61,63]	↓/↔↔							↓/↔ ↔↔	↔	↓/↔↔ ↔	↔		↓↓↓↓/ ↔↔	↓↓↓↓/↔ ↔
KK/Ay mice [64,65]	↑	↔	↔	↑	↔		↔						↓	
Ob/ob mice [67]											↓		↓	↓
Db/db mice [67,69]								↓			↓		↓/↔	↓
ZDSD rats [60,72,73,75]	↑↑	↑/↔	↔ ↔		↔		↔	↓/↔	↔	↓↓/↔ ↔	↓↓↓/↔	↔	↓	↓
WBN/Kob rats [12,76]					↓		↑	↓					↓	↓
TallyHo mice [74,77]	↑	↔	↓	↑	↔	↔↔	↔	↑/↔ ↔		↑↑/↔	↓	↔	↑↑/↔ ↔	↑/↔↔

1.4 Summary and Conclusions

Our understanding of mechanisms through which T1DM affects bone material properties is limited. Limited data on bone tissue from humans with T1DM showed higher mineral and AGE content and mechanical properties that may be similar to that of aging bone in a non-diabetic environment. In addition, tissue pentosidine content positively correlated with serum HbA1c, suggesting that AGE accumulation increases with worsening glycemic control. Further studies in larger cohorts are needed to quantitatively relate 1) glycemic control with compositional changes and 2) tissue-level compositional changes with mechanical properties across multiple levels of structural hierarchy.

Several mechanisms have been proposed to understand the effect of T2DM on bone tissue fragility [9,10,21], but the contribution of each mechanism to clinical fracture risk remains unknown. Recent studies on clinical specimens from humans with T2DM suggest that AGE accumulation and decreased bone remodeling [46] are important considerations in understanding the fragility of diabetic bone. Several mechanical measurements were made to investigate the fragility of bone tissue in human patients with T2DM; however, only a few studies directly investigated the association between mechanical properties and bone compositional properties. The sole study to date to characterize the composition and mechanical performance of cortical tissue found no relationship between AGEs and cyclic RPI outcomes [43]. On the other hand, significant relationships between composition and mechanical performance of cancellous bone have been reported in two studies. Specifically, AGEs were inversely correlated with post-yield properties [11,43], and mineral content was positively correlated with compressive stiffness and strength in cancellous tissue from the proximal femur [11]. These studies highlight the complex effects of T2DM on the mineral and matrix components of bone tissue, especially with regard to

AGE accumulation, and offer insight into how micro-scale material property changes may affect macro-scale mechanical integrity in a compartment-specific way.

Translating rodent studies to clinical outcomes remains challenging. No model holistically captures the changes in the material properties of bone observed in human studies associated with diabetes. For example, among T1DM rodent models, STZ-induced T1DM rats potentially reflect observed changes in the human T1DM studies. Among T2DM rodent models, obese mice and WBN/Kob rats reflect alterations in collagen properties, whereas ZDSD rats and TallyHo mice reflect changes in mineral composition observed in human studies. Interestingly, most of the rodent models of T2DM develop higher mineral content compared to controls, suggesting that bone turnover is consistently reduced regardless of the model-specific pathogenesis of T2DM. One major drawback in current rodent models is that most develop a reduced BMD, whereas in humans a normal to high BMD is observed. Additionally, a rodent model is needed to simulate conditions similar to T2DM in an older population, as no current model recapitulates all the characteristics of T2DM. Nevertheless, these models enable examination of the relationship of glycemic control and duration of disease with structural and material properties. Thus, these models can provide insight into the mechanisms of increased bone fragility in the human diabetic population.

Compliance with Ethical Standards

Conflict of Interest

Funding for this work was provided in part by NIH K01 AR064314 to ED. All authors declare no conflict of interest.

Human and Animal Rights and Informed Consent

This article does not contain any studies with human participants or animals performed by any of the authors.

1.5 References

Papers of particular interest, published recently, have been highlighted as: • Of importance •• Of major importance

1. Vestergaard P. Discrepancies in bone mineral density and fracture risk in patients with type 1 and type 2 diabetes - A meta-analysis. Osteoporos Int. 2007;18:427–44.

2. Janghorbani M, Van Dam RM, Willett WC, Hu FB. Systematic review of type 1 and type 2 diabetes mellitus and risk of fracture. Am J Epidemiol. 2007;166:495–505.

3. Shah VN, Carpenter RD, Ferguson VL, Schwartz A V. Bone health in type 1 diabetes. Curr Opin Endocrinol Diabetes Obes. 2018;25:231–6.

4. Schwartz A V., Vittinghoff E, Bauer DC, Hillier TA, Strotmeyer ES, Ensrud KE, et al. Association of BMD and FRAX score with risk of fracture in older adults with type 2 diabetes. JAMA - J Am Med Assoc. 2011;305:2184–92.

5. Bonds DE, Larson JC, Schwartz A V., Strotmeyer ES, Robbins J, Rodriguez BL, et al. Risk of fracture in women with type 2 diabetes: The women's health initiative observational study. J Clin Endocrinol Metab. 2006;91:3404–10.

6. Starup-Linde J, Frost M, Vestergaard P, Abrahamsen B. Epidemiology of Fractures in Diabetes. Calcif Tissue Int. Elsevier Inc.; 2017;100:109–21.

7. Schwartz A V. Epidemiology of fractures in type 2 diabetes. Bone. 2016;82:2–8.

8. Hough FS, Pierroz DD, Cooper C, Ferrari SL, IOF CSA Bone and Diabetes Working Group _. MECHANISMS IN ENDOCRINOLOGY: Mechanisms and evaluation of bone fragility in type 1 diabetes mellitus. Eur J Endocrinol. 2016;174:R127-38.

9. Napoli N, Chandran M, Pierroz DD, Abrahamsen B, Schwartz A V., Ferrari SL. Mechanisms of diabetes mellitus-induced bone fragility. Nat Rev Endocrinol. Nature Publishing Group; 2017;13:208–19.

10. Shanbhogue V V., Mitchell DM, Rosen CJ, Bouxsein ML. Type 2 diabetes and the skeleton: New insights into sweet bones. Lancet Diabetes Endocrinol. 2016;4:159–73.

11. •• Hunt H, Torres A, Palomino P, Marty E, Saiyed R, Cohn M, et al. Altered tissue composition, microarchitecture, and mechanical performance in cancellous bone from men with type 2 diabetes mellitus. J Bone Miner Res. 2019. This study relating compositional and mechanical properties found increased pentosidine and mineralization in men with T2DM, and showed that high concentrations of AGEs can increase fragility, especially for T2DM patients with low BV/TV.

12. Saito M, Fujii K, Mori Y, Marumo K. Role of collagen enzymatic and glycation induced cross-links as a determinant of bone quality in spontaneously diabetic WBN/Kob rats. Osteoporos Int. 2006;17:1514–23.

13. Vashishth D, Gibson GJ, Khoury JI, Schaffler MB, Kimura J, Fyhrie DP. Influence of nonenzymatic glycation on biomechanical properties of cortical bone. Bone. 2001;28:195–201.

14. Tang SY, Zeenath U, Vashishth D. Effects of non-enzymatic glycation on cancellous bone fragility. Bone. 2007;40:1144–51.

15. Yamagishi S-I. Role of advanced glycation end products (AGEs) and receptor for AGEs (RAGE) in vascular damage in diabetes. EXG. 2011;46:217–24.

16. Keenan HA, Maddaloni E. Bone Microarchitecture in Type 1 Diabetes: It Is Complicated. Curr Osteoporos Rep. Springer US; 2016;14:351–8.

17. Nilsson AG, Sundh D, Johansson L, Nilsson M, Mellström D, Rudäng R, et al. Type 2 Diabetes Mellitus Is Associated With Better Bone Microarchitecture But Lower Bone Material Strength and Poorer Physical Function in Elderly Women: A Population-Based Study. J Bone Miner Res. 2017;32:1062–71.

18. Kalaitzoglou E, Popescu I, Bunn RC, Fowlkes JL, Thrailkill KM. Effects of Type 1 Diabetes on Osteoblasts, Osteocytes, and Osteoclasts. Curr Osteoporos Rep. Springer US; 2016;14:310–9.

19. • Hygum K, Starup-Linde J, Harsløf T, Vestergaard P, Langdahl BL. Diabetes mellitus, a state of low bone turnover-a systematic review and meta-analysis. Eur J Endocrinol. 2017;176:R137–57. This extensive review of biochemical markers of bone formation and resorption in diabetes and found that low bone turnover is observed in both T1DM and T2DM conditions.

20. Zhukouskaya V V., Eller-Vainicher C, Shepelkevich AP, Dydyshko Y, Cairoli E, Chiodini I. Bone health in type 1 diabetes: Focus on evaluation and treatment in clinical practice. J Endocrinol Invest. Springer International Publishing; 2015;38:941–50.

21. Hamann C, Kirschner S, Günther KP, Hofbauer LC. Bone, sweet bone - Osteoporotic fractures in diabetes mellitus. Nat Rev Endocrinol. Nature Publishing Group; 2012;8:297–305.

22. •• Farlay D, Armas LAG, Gineyts E, Akhter MP, Recker RR, Boivin G. Nonenzymatic Glycation and Degree of Mineralization Are Higher in Bone from Fractured Patients with Type 1 Diabetes Mellitus. J Bone Miner Res. 2016;31:190–5. This is the only study to our knowledge to have assessed compositional properties in patients with T1DM and found increased AGE accumulation in patients with T1DM.

23. Fleischli JG, Laughlin TJ, Lavery LA, Shah B, Lanctot D, Agrawal CM, et al. The effects of diabetes mellitus on the material properties of human metatarsal bones. J Foot Ankle Surg. 1998;37:195–8.

24. Fleischli JG, Laughlin TJ, Athanasiou K, Lanctot DR, Lavery L, Wang X, et al. Effect of Diabetes Mellitus on the Material Properties of the Distal Tibia. J Am Pod Med Assoc. 2014;96:91–5.

25. Lenzen S. The mechanisms of alloxan- and streptozotocin-induced diabetes. Diabetologia. 2008;51:216–26.

26. •• Fajardo RJ, Karim L, Calley VI, Bouxsein ML. A review of rodent models of type 2 diabetic skeletal fragility. J Bone Miner Res. 2014;29:1025–40. This extensive review discusses the effect of T2DM on the skeletal phenotype of different rodent models.

27. Paschalis EP, Verdelis K, Doty SB, Boskey AL, Mendelsohn R, Yamauchi M. Spectroscopic characterization of collagen cross-links in bone. J Bone Miner Res. 2001;16:1821–8.

28. Oliveira Limirio PHJ, Da Rocha HA, De Morais RB, Hiraki KRN, Balbi APC, Soares PBF, et al. Influence of hyperbaric oxygen on biomechanics and structural bone matrix in type 1 diabetes mellitus rats. PLoS One. 2018;13.

29. Bozkurt O, Bilgin MD, Evis Z, Pleshko N, Severcan F. Early Alterations in Bone Characteristics of Type i Diabetic Rat Femur: A Fourier Transform Infrared (FT-IR) Imaging Study. Appl Spectrosc. 2016;70:2005–15.

30. Donmez BO, Unal M, Ozdemir S, Ozturk N, Oguz N, Akkus O. Effects of losartan treatment on the physicochemical properties of diabetic rat bone. J Bone Miner Metab. 2017;35:161–70.

31. Silva MJ, Brodt MD, Lynch MA, McKenzie JA, Tanouye KM, Nyman JS, et al. Type 1 diabetes in young rats leads to progressive trabecular bone loss, cessation of cortical bone growth, and diminished whole bone strength and fatigue life. J Bone Miner Res. 2009;24:1618–27.

32. Mansur SA, Mieczkowska A, Bouvard B, Flatt PR, Chappard D, Irwin N, et al. Stable Incretin Mimetics Counter Rapid Deterioration of Bone Quality in Type 1 Diabetes Mellitus. J Cell Physiol. 2015;230:3009–18.

33. Mieczkowska A, Mansur SA, Irwin N, Flatt PR, Chappard D, Mabilleau G. Alteration of the bone tissue material properties in type 1 diabetes mellitus: A Fourier transform infrared microspectroscopy study. Bone. 2015;76:31–9.

34. Facchini DM, Yuen VG, Battell ML, McNeill JH, Grynpas MD. The effects of vanadium treatment on bone in diabetic and non-diabetic rats. Bone. 2006;38:368–77.

35. Makowski AJ, Patil CA, Mahadevan-Jansen A, Nyman JS. Polarization control of Raman spectroscopy optimizes the assessment of bone tissue. J Biomed Opt. International Society for Optics and Photonics; 2013;18:055005.

36. Taylor EA, Lloyd AA, Salazar-Lara C, Donnelly E. Raman and Fourier Transform Infrared (FT-IR) Mineral to Matrix Ratios Correlate with Physical Chemical Properties of Model Compounds and Native Bone Tissue. Appl Spectrosc. 2017;71:2404–10.

37. Nyman JS, Even JL, Jo CH, Herbert EG, Murry MR, Cockrell GE, et al. Increasing duration of type 1 diabetes perturbs the strength-structure relationship and increases brittleness of bone. Bone. 2011;48:733–40.

38. Zhang H, Gan L, Zhu X, Wang J, Han L, Cheng P, et al. Moderate-intensity 4 mT static magnetic fields prevent bone architectural deterioration and strength reduction by stimulating bone formation in streptozotocin-treated diabetic rats. Bone. 2018;107:36–44.

39. Rubin MR, Paschalis EP, Poundarik A, Sroga GE, McMahon DJ, Gamsjaeger S, et al. Correction: Advanced glycation endproducts and bone material properties in type 1 diabetic mice. PLoS One. 2016;11:1–14.

40. Epstein PN, Overbeek PA, Means AR. Calmodulin-induced early-onset diabetes in transgenic mice. Cell. 1989;58:1067–73.

41. Thrailkill KM, Lumpkin CK, Bunn RC, Kemp SF, Fowlkes JL. Is insulin an anabolic agent in bone? Dissecting the diabetic bone for clues. Am J Physiol Endocrinol Metab. 2005;289:E735-45.

42. Lecka-Czernik B. Safety of Antidiabetic Therapies on Bone. Clin Rev Bone Miner Metab. 2013;11:49–58.

43. •• Karim L, Moulton J, Van Vliet M, Velie K, Robbins A, Malekipour F, et al. Bone microarchitecture, biomechanical properties, and advanced glycation end-products in the

proximal femur of adults with type 2 diabetes. Bone. Elsevier; 2018;114:32–9. This is the first study to examine compositional and mechanical properties of bone from humans with T2DM and found reduced resistance to creep indentation in cortical bone from patients with T2DM.

44. Bucknell A, King KB, Oren TW, Botolin S, Williams A. Arthroplasty in veterans: Analysis of cartilage, bone, serum, and synovial fluid reveals differences and similarities in osteoarthritis with and without comorbid diabetes. J Rehabil Res Dev. 2012;48:1195.

45. Pritchard JM, Papaioannou A, Tomowich C, Giangregorio LM, Atkinson SA, Beattie KA, et al. Bone mineralization is elevated and less heterogeneous in adults with type 2 diabetes and osteoarthritis compared to controls with osteoarthritis alone. Bone. Elsevier Inc.; 2013;54:76–82.

46. Manavalan JS, Cremers S, Dempster DW, Zhou H, Dworakowski E, Kode A, et al. Circulating Osteogenic Precursor Cells in Type 2 Diabetes Mellitus. J Clin Endocrinol Metab. 2012;97:3240–50.

47. •• Farr JN, Drake MT, Amin S, Melton LJ, McCready LK, Khosla S. In vivo assessment of bone quality in postmenopausal women with type 2 diabetes. J Bone Miner Res. 2014;29:787–95. This comprehensive assessment of geometric and microarchitectural properties in women with T2DM demonstrated that bone material strength index decreased with 10-year HbA1c.

48. Furst JR, Bandeira LC, Fan WW, Agarwal S, Nishiyama KK, Mcmahon DJ, et al. Advanced glycation endproducts and bone material strength in type 2 diabetes. J Clin Endocrinol Metab. 2016;101:2502–10.

49. Arnold M, Zhao S, Ma S, Giuliani F, Hansen U, Cobb JP, et al. Microindentation – a tool for measuring cortical bone stiffness? Bone Jt Res. 2017;6:542–9.

50. Poundarik AA, Wu PC, Evis Z, Sroga GE, Ural A, Rubin M, et al. A direct role of collagen glycation in bone fracture. J Mech Behav Biomed Mater. 2015;50:82–92.

51. Karim L, Tang SY, Sroga GE, Vashishth D. Differences in non-enzymatic glycation and collagen cross-links between human cortical and cancellous bone. Osteoporos Int. 2013;24:2441–7.

52. Schmidt FN, Zimmermann EA, Campbell GM, Sroga GE, Püschel K, Amling M, et al. Assessment of collagen quality associated with non-enzymatic cross-links in human bone using Fourier-transform infrared imaging. Bone. 2017;97:243–51.

53. Willett TL, Sutty S, Gaspar A, Avery N, Grynpas M. In vitro non-enzymatic ribation reduces post-yield strain accommodation in cortical bone. Bone. Elsevier Inc.; 2013;52:611–22.

54. Marin C, Papantonakis G, Sels K, Van Lenthe GH, Falgayrac G, Vangoitsenhoven R, et al. Unraveling the compromised biomechanical performance of type 2 diabetes- and Roux-en-Y gastric bypass bone by linking mechanical-structural and physico-chemical properties. Sci Rep. Springer US; 2018;8:1–12.

55. Ionova-Martin SS, Wade JM, Tang S, Shahnazari M, Ager JW, Lane NE, et al. Changes in cortical bone response to high-fat diet from adolescence to adulthood in mice. Osteoporos Int. 2011;22:2283–93.

56. Kerckhofs G, Durand M, Vangoitsenhoven R, Marin C, Van Der Schueren B, Carmeliet G, et al. Changes in bone macro-and microstructure in diabetic obese mice revealed by high resolution microfocus X-ray computed tomography. Sci Rep. Nature Publishing Group; 2016;6:1–13.

57. Ionova-Martin SS, Do SH, Barth HD, Szadkowska M, Porter AE, Ager JW, et al. Reduced size-independent mechanical properties of cortical bone in high-fat diet-induced obesity. Bone. Elsevier Inc.; 2010;46:217–25.

58. Clark JB, Palmer CJ, Shaw WN. The diabetic Zucker fatty rat. Proc Soc Exp Biol Med. 1983;173:68–75.

59. Fu C, Zhang X, Ye F, Yang J. High Insulin Levels in KK-Ay Diabetic Mice Cause Increased Cortical Bone Mass and Impaired Trabecular Micro-Structure. Int J Mol Sci. 2015;16:8213–26.

60. Reinwald S, Peterson RG, Allen MR, Burr DB. Skeletal changes associated with the onset of type 2 diabetes in the ZDF and ZDSD rodent models. Am J Physiol Endocrinol Metab. 2009;296:E765-74.

61. Prisby RD, Swift JM, Bloomfield SA, Hogan HA, Delp MD. Altered bone mass, geometry and mechanical properties during the development and progression of type 2 diabetes in the Zucker diabetic fatty rat. J Endocrinol. 2008;199:379–88.

62. Pereira M, Gohin S, Lund N, Hvid A, Smitham PJ, Oddy MJ, et al. Sclerostin does not play a major role in the pathogenesis of skeletal complications in type 2 diabetes mellitus. Osteoporos Int. Osteoporosis International; 2017;28:309–20.

63. Hamann C, Goettsch C, Mettelsiefen J, Henkenjohann V, Rauner M, Hempel U, et al. Delayed bone regeneration and low bone mass in a rat model of insulin-resistant type 2 diabetes mellitus is due to impaired osteoblast function. Am J Physiol Metab. 2011;301:E1220–8.

64. Xu F, Dong Y, Huang X, Li M, Qin L, Ren Y, et al. Decreased osteoclastogenesis, osteoblastogenesis and low bone mass in a mouse model of type 2 diabetes. Mol Med Rep. 2014;10:1935–41.

65. Hunt HB, Pearl JC, Diaz DR, King KB, Donnelly E. Bone Tissue Collagen Maturity and Mineral Content Increase With Sustained Hyperglycemia in the KK-Ay Murine Model of Type 2 Diabetes. J Bone Miner Res. 2018;33:921–9.

66. Takagi S, Miura T, Yamashita T, Ando N, Nakao H, Ishihara E, et al. Characteristics of Diabetic Osteopenia in KK-Ay Diabetic Mice. Biol Pharm Bull. 2012;35:438–43.

67. Ealey KN, Fonseca D, Archer MC, Ward WE. Bone abnormalities in adolescent leptin-deficient mice. Regul Pept. 2006;136:9–13.

68. Williams GA, Callon KE, Watson M, Costa JL, Ding Y, Dickinson M, et al. Skeletal phenotype of the leptin receptor-deficient db/db mouse. J Bone Miner Res. 2011;26:1698–709.

69. Huang L, You YK, Zhu TY, Zheng LZ, Huang XR, Chen HY, et al. Validity of leptin receptor-deficiency (db/db) type 2 diabetes mellitus mice as a model of secondary osteoporosis. Sci Rep. Nature Publishing Group; 2016;6:1–7.

70. Kim JH, Sen Ś, Avery CS, Simpson E, Chandler P, Nishina PM, et al. Genetic Analysis of a New Mouse Model for Non-Insulin-Dependent Diabetes. Genomics. 2001;74:273–86.

71. Kutscher CL, Miller M, Schmalbach NL. Renal deficiency associated with diabetes insipidus in the SWR/J mouse. Physiol Behav. 1975;14:815–8.

72. Hammond MA, Gallant MA, Burr DB, Wallace JM. Nanoscale changes in collagen are reflected in physical and mechanical properties of bone at the microscale in diabetic rats. Bone. Elsevier Inc.; 2013;60:26–32.

73. Creecy A, Uppuganti S, Merkel AR, O'Neal D, Makowski AJ, Granke M, et al. Changes in the Fracture Resistance of Bone with the Progression of Type 2 Diabetes in the ZDSD Rat. Calcif Tissue Int. Springer US; 2016;99:289–301.

74. Creecy A, Uppuganti S, Unal M, Clay Bunn R, Voziyan P, Nyman JS. Low bone toughness in the TallyHO model of juvenile type 2 diabetes does not worsen with age. Bone. Elsevier Inc.; 2018;110:204–14.

75. Gallant MA, Brown DM, Organ JM, Allen MR, Burr DB. Reference-point indentation correlates with bone toughness assessed using whole-bone traditional mechanical testing. Bone. Elsevier Inc.; 2013;53:301–5.

76. Igarashi C, Maruyama T, Ezawa I, Takei I, Saruta T. WBN/Kob rat: a new model of spontaneous diabetes, osteopenia and systemic hemosiderin deposition. Bone Miner. 1994;27:133–44.

77. Devlin MJ, Van Vliet M, Motyl K, Karim L, Brooks DJ, Louis L, et al. Early-onset type 2 diabetes impairs skeletal acquisition in the male TALLYHO/JngJ mouse. Endocrinology. 2014;155:3806–16.

CHAPTER 2

INCREASED ADVANCED GLYCATION ENDPRODUCTS, STIFFNESS, AND HARDNESS IN ILIAC CREST BONE FROM POSTMENOPAUSAL WOMEN WITH TYPE 2 DIABETES MELLITUS

2.1 Introduction

Individuals with type 2 diabetes mellitus (T2DM) have an increased risk of bone fracture despite normal to high bone mineral density (BMD) compared to non-diabetic individuals.[1,2] The increased fracture risk persists even after adjusting for the greater BMD, body mass index (BMI), and risk of falls typically observed in individuals with T2DM.[3–6] In contrast, individuals with impaired glucose tolerance (IGT) have a lower or similar risk of fracture compared to individuals with normal glucose tolerance (NGT).[7,8] This reduced fracture risk in individuals with IGT may be explained by greater BMD.[7,9] However, individuals with T2DM have higher BMD compared to individuals with IGT or NGT[7] and yet have a greater risk of fracture. Therefore, while maintaining BMD and controlling for risk factors such as falls, fat mass, and smoking, the progression from IGT to T2DM may lead to deleterious metabolic or biochemical changes that degrade bone tissue properties.[9–12]

The mechanisms responsible for increased fracture risk in individuals with impaired glucose metabolism are not well understood. Two hypothesized mechanisms by which bone composition and material properties may be altered in individuals with T2DM include impaired bone remodeling and accumulation of advanced glycation endproducts (AGEs).[10,11] Reduced bone formation in individuals with T2DM was observed in histomorphometric studies[13,14] and corroborated by lower serum levels of bone formation and resorption markers.[15,16] Similar

trends of bone turnover markers were observed in pre-diabetic individuals.[17] Reduced bone remodeling results in microdamage accumulation and a loss in toughness with homogenization of microscale and nanoscale material properties.[18–21] Reduced remodeling in addition with impaired osteoblast[22] and osteoclast[23] function with progressive glycemic derangement may allow longer secondary mineralization. Increased mineral content stiffens the tissue and has a positive effect on bone strength.[24] Reduced remodeling can therefore have both beneficial and detrimental effects on bone strength.

In addition, hyperglycemia in individuals with T2DM can lead to formation of AGEs via non-enzymatic glycation of amino acid residues on collagen.[25–27] These AGEs accumulate in bone with age[28,29] and embrittle the tissue.[25,30] On the other hand, enzymatic crosslinks are formed in a controlled manner regulated by lysyl oxidase and increase whole bone strength.[31] Pyridinoline, a mature enzymatic crosslink was lower in trabecular bone from men with T2DM compared to non-DM men.[25] The mechanism for reduced enzymatic crosslinking and its effect on bone strength in individuals with T2DM is unknown. Impaired osteoblast function in individuals with T2DM[22] which regulate lysyl oxidase secretion can lead to reduced enzymatic crosslinking. Additionally, excessive non-enzymatic crosslinking may reduce the bonding sites for the formation of enzymatic crosslinks. Therefore, a detrimental combination of increased AGEs, and consequently reduced enzymatic crosslinking is a potential mechanism for increased fracture risk in individuals with T2DM.

Recent studies of clinical specimens from individuals with T2DM reported differences in bone compositional and material properties. Bone from individuals with T2DM had greater 1) concentrations of total fluorescent AGEs (fAGEs) in cortical but not trabecular bone;[25,26] 2) concentrations of the specific crosslinking AGE, pentosidine;[25,27] and 3) bone mineral

content, all consistent with reduced remodeling.[25,32] These compositional changes had both beneficial and detrimental effects on bone mechanical performance. Regression analyses showed that higher mineral content increases structural strength and stiffness, whereas higher AGE content reduces post-yield toughness in cancellous bone.[25] Overall, the cancellous bone strength and stiffness was comparable or higher in individuals with T2DM predominantly due to higher bone volume fraction. However, the tissue from the individuals without the protective effect of higher bone volume fraction was more brittle due to greater concentrations of AGEs.

However, numerous gaps remain in our understanding of the factors that drive fragility in T2DM, and the composition and mechanical properties of bone tissue in individuals with IGT are unknown. In an obese rodent model that develops pre-diabetes, greater total fAGEs were observed compared to the lean controls, indicating that AGE accumulation in bone matrix begins in a prediabetic stage.[33,34] This result requires confirmation in human populations. Furthermore, lower microscale resistance of cortical bone to *in vivo* impact indentation and *ex vivo* cyclic reference point indentation were observed in individuals with T2DM.[26,35–37] However, the changes in bone microstructure or composition responsible for these differences are unknown, and the outcomes require further validation to associate with tissue material properties. Furthermore, existing studies have focused primarily on men[25,27] and subjects with T2DM sufficiently well controlled for elective total hip arthroplasty.[25,26] Cohorts with a wide range of disease severity are required to understand the progression of the changes in bone material properties from normal glucose tolerance to overt T2DM.

The goal of our study was to understand how progressive glycemic derangement affects the composition and mechanical properties of bone matrix. We enrolled postmenopausal women with normal glucose tolerance (NGT), impaired glucose tolerance (IGT) and overt T2DM. Our

approach included (1) measurement of the nanomechanical and compositional properties of cortical and trabecular bone from individuals with and without T2DM, (2) assessment of the spatial distribution of AGEs and collagen organization in the groups, and (3) assessment of the quantity of enzymatic and non-enzymatic collagen crosslinks in all the groups. We hypothesized that (1) individuals with T2DM have higher bone mineral content, which results in stiffer and harder tissue; (2) AGE content increases from a pre-diabetic stage and negatively correlates with enzymatic crosslinks

2.2 Methods

2.2.1 Study Cohort

Post-menopausal women were recruited at Johns Hopkins University as described in a previous study.[38] The participants were allocated to three groups 1) normal glucose tolerance (NGT, n = 35), if blood glucose level after 2-hour 75-g oral glucose tolerance test (OGTT) was less than 140 mg/dL; 2) impaired glucose tolerance (IGT, n = 26), if blood glucose level after OGTT was between 140 mg/dL and 199 mg/dL; and 3) T2DM (n = 23), if diagnosed with T2DM and on insulin therapy. Women with T2DM but not on insulin therapy were excluded from the T2DM group to study the effects of severe T2DM on bone. Further, women with type 1 diabetes, a history of fragility fracture, osteoporosis, other metabolic bone diseases (Paget's, hyperparathyroidism, vitamin D deficiency), on medications known to affect bone metabolism were excluded from this study to eliminate potential confounding effects. Women using medications known to affect bone (glucocorticoids, estrogen, anti-epileptic drugs, thiazolidinediones, aromatase inhibitors, osteoporosis therapies) were also excluded.

All participants provided informed consent, and all study procedures were approved by

the Johns Hopkins Medicine Institutional Review Board. The participants completed five visits: 1) initial screening to assess medical history and administer OGTT to determine glycemic control; 2) secondary screening to obtain samples for blood and urine analyses, including urine protein, markers of bone resorption and formation, 25-hydroxy vitamin D, hemoglobin A1c (HbA1c), parathyroid hormone (PTH) and a complete metabolic panel; 3) baseline visit to instruct participants how to administer demeclocycline double-labeling and how to prepare for bone biopsy; 4) bone biopsy visit to obtain iliac crest sample; and 5) final visit to remove sutures and address follow-up questions. Participants were compensated for each visit. Participants were instructed to take two courses of demeclocycline, each course lasting three days. A twelve-day gap was given between the two courses, and the biopsy was obtained five days after the second course. Biopsies were stored in ethanol prior to tissue processing.

2.2.2 Nanoindentation

From an initial power analysis, fourteen samples with lowest CTx were chosen from each group (NGT and T2DM) to detect a 10% difference in the modulus. The samples with lowest CTx were chosen to determine the effects of reduced remodeling in individuals with T2DM. The biopsies were dehydrated using organic solvents and embedded in poly methyl methacrylate. The longitudinal sections were anhydrously polished with a series of abrasive grit papers and alumina slurry to achieve an RMS roughness less than 20 nm[39], as assessed by atomic force microscopy scans of at least four 5 x 5 μm^2 areas per sample. Specimens were rehydrated in Hank's balanced salt solution (HBSS) for three hours prior to testing.

A nanoindenter (TriboIndenter, Hysitron) with a Berkovich diamond tip was used to collect force vs. displacement data. The tip was loaded into the sample at 100 μN/s, held at the maximum load of 1000 μN for 30s, and unloaded at 100 μN/s, which produced indentations with

contact depths ~ 200 nm. Indentation modulus and hardness were calculated from the unloading portion of the force-displacement curve as previously described.[39,40]

Both cortical and trabecular bone were characterized with nanoindentation. At least 30 indents were made in cortical and trabecular bone to account for the heterogeneity in the tissue.[41,42] In cortical bone, two osteonal and two interstitial regions per sample were characterized. Two osteons were randomly chosen, and fifteen equidistant indents were placed across the total width of each osteon. Next, two randomly chosen interstitial regions were characterized with 2×2 grids of indents with 5 μm grid spacing. In trabecular bone, two trabeculae with fluorescent labels of bone formation (Supplementary Figure 2.1) were randomly chosen to study the effect of tissue age on material properties. In each trabecula, three sub-regions were characterized (Figure 2.1B, 2.1C, 2.1D). Five indents, spaced 5 μm apart, were made along a line perpendicular to the trabecular edge 1) at the formation label (the "label sub-region"), representing newly formed bone (<24 d old) and 2) at the opposite trabecular edge without formation labels (the "edge sub-region"), representing bone >24 days old; another five equidistant indents were made along the same line in the center of the trabecula from 30% to 70% the width of trabecula (the "center sub-region") (Figure 2.1B).

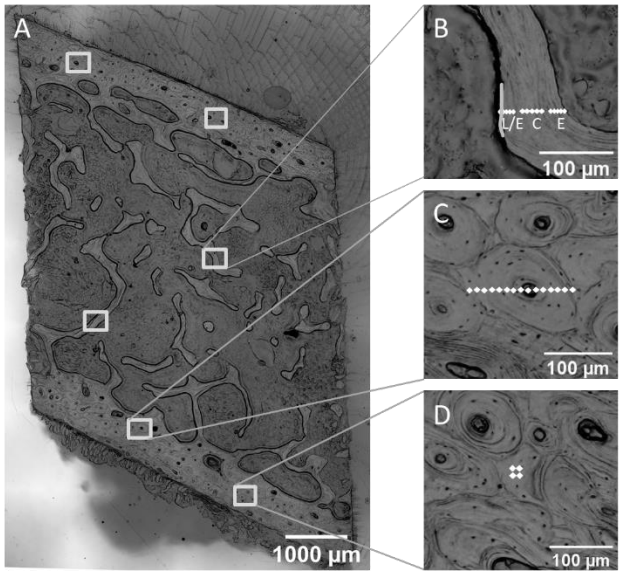

Figure 2.1. (A) Representative stitched optical image of an iliac crest biopsy showing the regions of interest for nanoindentation. Regions of interest are highlighted with rectangles: (B) trabecular bone; (C) cortical osteonal bone; (D) interstitial bone. Inset images schematically depict indentations: each rhombus represents an indentation (not to scale). The trabecular regions depict indentations on fluorochrome labels in label (L), center (C) and edge (E) sub-regions. The indents that fall beyond the fluorochrome label are marked as edge sub-region.

2.2.3 Raman Spectroscopy

Compositional properties of cortical and trabecular bone from the subset of samples that underwent nanoindentation were characterized using Raman spectroscopy. Spectra were acquired using a confocal Raman imaging system (Alpha300R, WITec) with a ~70mW 785 nm laser source focused through a 50×, 0.55 numerical aperture (NA) objective. Each spectrum was averaged from 10 accumulations each obtained with a 6-second integration time.

In cortical bone, at least three osteonal and three interstitial regions were characterized to spatially match the regions characterized by nanoindentation, and the rest of the regions were randomly selected. Three spectra, equidistantly spaced, were collected along a line spanning the

radius of each osteon and three spectra spaced 10 µm apart were collected in each interstitial region. In trabecular bone, at least three trabeculae were characterized per sample. Spectra were collected along lines parallel to the surface of each trabecula, at three points spaced 10 µm apart in each of three sub-regions: 1) Label: the edge of the trabecula with the bone formation label; 2) Edge: the edge of trabecula without formation label, and 3) Center: the center of the trabecula.

The background fluorescence was subtracted from the spectra using a chemical imaging software (Project FIVE 5.2, WITec). The PMMA contribution to the bone spectra was subtracted. Four outcomes (Table 2.1) were determined by direct integration using a custom code (MATLAB, MathWorks). Pyridinoline content was calculated by peak fitting the Amide I region using a spectroscopy software (GRAMS/AI, Thermo Fisher Scientific). The Amide I region was resolved into four Gaussian sub-bands centered at 1610, 1630, 1660, and 1690.[43]

Table 2.1. Raman outcomes and their corresponding vibrational mode or peak area ratio along with the integration ranges. FWHM: full width at half maximum.

Raman outcome	**Vibrational mode or peak area ratio**	**Integration ranges (**cm^{-1}**)**	**References**
Mineral:Matrix ratio (M:M)	$\nu_2 PO_4$ / Amide III	(410-460) / (1215-1300)	[44]
Mineral crystallinity / maturity (XST)	1/FWHM of $\nu_1 PO_4$ (~ 960 cm^{-1})	N/A	[45]
Carbonate:Phosphate ratio (C:P)	$\nu_1 CO_3$ / $\nu_2 PO_4$	(1050-1100) / (410-460)	[46]
Glycosaminoglycan (GAG)	CH_3 / Amide III	(1365-1390) / (1215-1300)	[47]
Pyridinoline (PYD)	Pyridinoline / Amide I	1660 / (1616-1720)	[48]

2.2.4 Confocal/Multiphoton Imaging (MPM)

All the samples from the NGT and T2DM groups were imaged with confocal/multiphoton microscopy to collect spatially resolved images of fluorescent AGEs and collagen alignment in cortical and trabecular bone. Three cortical and trabecular regions each 425 x 425 μm^2 previously characterized by nanoindentation and Raman spectroscopy were also characterized with multiphoton microscopy.

The confocal/MPM system (LSM 880, Zeiss) comprises an upright microscope (Axio Examiner.Z1, Zeiss) and multiple laser lines, including the Diode 405-30 unit used for confocal imaging and fully spectrally-resolvable emission channels. The system also has a fully integrated Ti:Sapphire (Mai Tai, Spectra Physics) multiphoton excitation source with automated tuning and pulse dispersion control from 700 nm-1000 nm. Second harmonic generation (SHG) imaging was done with a non-descanned filter-based unit. Incident light was focused on the samples using either a 20X, 1.0 NA dipping lens or 40X, 1.1 NA lens with a 0.17-mm-thick coverslip on the sample surface. HBSS was used as the immersion medium for both lenses. To account for different objectives, the power of the incident lasers was scaled to maintain similar fluorescence and SHG intensities at the specimen surface.[49] Otherwise, the power and all settings were kept the same between samples.

Confocal imaging was used to obtain semi-quantitative spatial distributions of AGE content in cortical and trabecular bone. Images of fluorescent AGEs were obtained by focusing the 405 nm laser on the sample and collecting fluorescence over 430-450 nm. In each region, fluorescence was collected from one 1-μm-thick optical section to minimize photobleaching by adjusting the pinhole aperture.

The endogenous fluorescence from the bone was normalized to that of cascade blue dye (Cascade Blue hydrazide, Trisodium Salt (C-687), Thermo Fisher Scientific), which has a similar

excitation-emission profile to AGEs in collagen.[50] The fluorescence intensities of serially diluted calibration standards of 100 μM C-687 dye in deionized water were measured with the same system settings used to obtain fAGE images. The fluorescence intensity at each pixel was converted to fAGE concentration using calibration curves made from the standards. The mean and the standard deviation of the normalized fluorescence intensity were calculated for each image.

Collagen organization was assessed from SHG images collected from the same regions. Second-harmonic was generated using a circularly polarized laser providing <100 fs pulses at 80 MHz tuned to a wavelength of 780 nm. The incident laser was circularly polarized using a Berek variable waveplate (5540, New Focus) to generate second-harmonic from collagen in all orientations. First order (mean, standard deviation) and second order (Table 2.2) statistical parameters of collagen organization were calculated from the images.[51]

Table 2.2. Texture analysis outcomes and their description calculated from gray level co-occurrence matrix (GLCM). P(i,j) is the value of the element (i,j) of the symmetrical GLCM; N is the matrix size (N × N); μ is the mean; and σ^2 is the variance of the intensities of all pixels in the relationships that contributed to the GLCM.

Parameter	Description
$Uniformity = \sum_{i=0}^{N-1}\sum_{j=0}^{N-1} P(i,j)^2$	Measures the uniformity of the gray level distribution of the image. Low values are associated with a uniform image.
$Homogeneity = \sum_{i=0}^{N-1}\sum_{j=0}^{N-1} \frac{P(i,j)}{1+(i-j)^2}$	Measures the smoothness of the gray level distribution of the image. Higher values are associated with denser or thicker collagen fibers in the SHG image.

$Contrast = \sum_{i=0}^{N-1}\sum_{j=0}^{N-1}(i-j)^2 P(i,j)$	Measures large differences in gray level in the image.
$Correlation = \sum_{i=0}^{N-1}\sum_{j=0}^{N-1} P(i,j)\frac{(i-\mu)(j-\mu)}{\sigma^2}$	Measures the dependence of gray levels on neighboring pixels. High values indicate a periodic collagen structure.
$Entropy = -\sum_{i=0}^{N-1}\sum_{j=0}^{N-1} P(i,j)\log(P(i,j))$	Measures the randomness of gray levels of the image. Low entropy indicates uniformity and high entropy indicates that bright elements are present on the homogeneous background.

2.2.5 High Performance Liquid Chromatography

High performance liquid chromatography (HPLC) was used to determine the quantity of AGE pentosidine and mature enzymatic crosslinks, pyridinoline (Pyd) and deoxypyridinoline (Dpd). All the samples in NGT, IGT and T2DM were characterized using HPLC. The biopsies were de-embedded from PMMA by agitating in methyl acetate (4 days, new solution every 24 hours) and 100% acetone (24 hours). After de-embedding, the biopsies were washed in 100% ethanol (24 hours) and de-fatted in isopropyl ether (15 min × 3). The tissues were sectioned into cortical and trabecular compartments for separate analysis of each compartment. The separated tissues were rinsed in deionized water, lyophilized, and hydrolyzed in 6 N HCl at 110ºC for 20 hours. Hydrolysates equivalent to 5 mg of dry bone were dried in a vacuum centrifuge (Savant SPD131DDA SpeedVac Concentrator, Thermo Fisher Scientific) connected to a refrigerated vapor trap (RVT5105, Thermo Fisher Scientific). Dried powders were resuspended in an internal standard solution (10 nM pyridoxine and 2.4 µM homoarginine) and filtered with 0.45 µm syringe filter. The filtered solutions were diluted 1:5 with 10% acetonitrile (v/v) and 0.5%

heptafluorobutyric acid (v/v).

The crosslinks were separated using two isocratic steps[52] by injecting the diluted solution into a 50 mm long column (XBridge C18, Waters Corporation) integrated in a programmable HPLC system (Alliance e2695, Waters Corporation) attached to a UV-Vis detector (e2475, Waters Corporation). A linear calibration curve was obtained for each HPLC run using serially diluted (6 levels; 1:2 dilution in HPLC water) calibration standard containing pentosidine (Case Western Reserve University), Pyd, and Dpd (8004, Quidel).

The crosslinks concentrations were normalized by collagen concentrations determined by hydroxyproline concentration from amino acid analysis. For this analysis, the diluted sample from crosslink analysis was further diluted 1:50 with 6 mM homoarginine in 0.1 M borate buffer (pH 11.4). For improved detection, this solution was derivatized using 6mM fluorenylmethyloxycarbonyl chloride for 40 min, and excess reagents and byproducts were extracted three times using pentane. After derivatization, the samples were diluted using 25% (v/v) acetonitrile in 0.25 M boric acid (pH 5.5). The amino acids were separated using the same column and system.[53] A linear calibration curve was obtained for each amino acid run using serially diluted (6 levels; 1:2 dilution in HPLC water) calibration standard containing purified hydroxyproline (Sigma-Aldrich) and 6 μM homoarginine in 0.1M borate buffer (pH 11.4).

2.2.6 Fluorometric Assay for Total AGEs

Fluorometric assay was used to mesaure total fluorescent AGE (fAGE) content in cortical and trabecular bone from all the groups.[25] The bone hydrolysates prepared for HPLC were diluted with deionized water to 2 μg bone/mL solution. Fluorescence from quinine standards (Sigma-Aldrich) was used to quantify the fluorescence from bone. The fluorescence of diluted bone hydrolysate and the quinine standards were measured in a 96-well plate using a multimode

microplate reader (Synergy H1, BioTek) at an excitation of 360 nm and an emission of 460 nm. A colorimetric assay of hydroxyproline was used to determine collagen content to normalize the bulk fluorescence. For the bone tissue samples, the hydrolysate measured for bulk fluorescence was diluted with deionized water to 0.2 µg bone/mL. To initiate the reaction, chloramine-T was added to the hydroxyproline standards and the diluted sample hydrolysates. The standards and samples were incubated for 20 minutes at room temperature, then 3.15 M perchloric acid was added to stop the reaction. After sitting 5 minutes at room temperature, p-dimethylaminobenzaldehyde was added. The standards and samples were incubated at 60°C in a water bath for 20 minutes, then cooled in cold water in darkness to room temperature. The absorbance of the specimens and standards was measured at a wavelength of 570 nm in a 96-well plate multimode microplate reader. Total fAGEs are reported in units of ng quinine fluorescence/mg collagen.

2.2.2 Statistical Analysis

All statistical analyses were done using a commercial software (JMP Pro 14, SAS Institute). All the outcomes were tested for normality using Shapiro-Wilk tests. Log transformation was performed if the data was not normally distributed. Linear mixed effects models were used to assess the effects of study group and tissue age on the characterization outcomes in cortical and trabecular bone. The fixed effects were the study group (NGT, IGT, T2DM), tissue sub-region (cortical bone: osteonal, interstitial; trabecular bone: label, edge, center and the interaction between study group and tissue sub-region. The random effects were the patient ID and the region of interest (two or three regions depending on the method) to account for repeated measures and non-independence in the data. The p-values for pair-wise comparisons were obtained from Tukey's HSD test. Standard least squares regression modeling was performed to

understand the effect of composition on mechanical properties. Significance was set as $p < 0.05$ for all the outcomes. Data is presented as estimated mean ± standard deviation or as box and whisker plots on which the p-values are the adjusted p-values from the Tukey HSD tests.

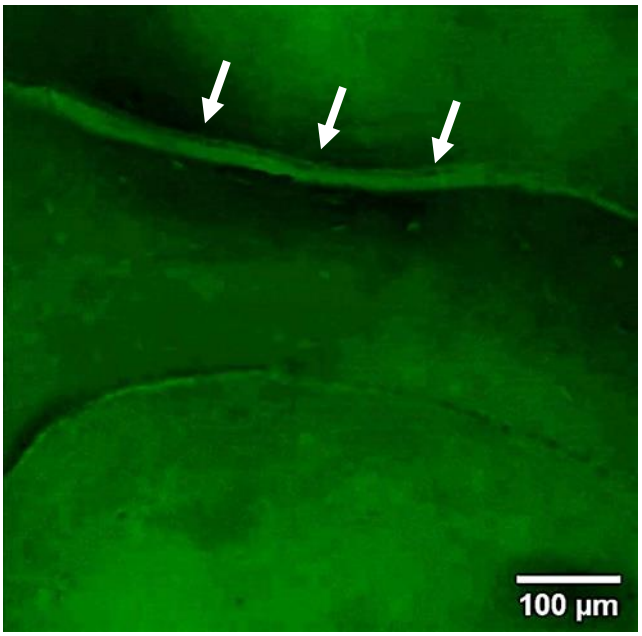

Supplementary Figure 2.1. Trabecula showing a fluorochrome label (indicated by white arrows) representing newly formed bone (< 28 days old). The optical image was obtained using a Red+Blue filter. Double labels could not be resolved in the thick embedded bone.

2.3 Results

2.3.2 Patient Characteristics

Participant characteristics, reported previously for this cohort[38], are summarized in Table 2.3. Average age was not different among the groups. BMI in individuals with IGT and T2DM was greater compared to individuals with NGT (+16% vs. IGT, $p = 0.019$; +23% vs. T2DM, $p < 0.001$) but did not differ between IGT and T2DM groups. Average value of glycated hemoglobin (HbA1C) in individuals with T2DM (9.1% ± 2.2%) was greater than individuals with NGT (5.8% ± 0.3%) and IGT (6.0% ± 0.4%) (+59% vs. NGT, $p = 0.008$; +51% vs. IGT, $p < 0.001$)

but did not differ between IGT and NGT groups.

The markers of bone turnover were lower in individuals with T2DM compared to individuals with NGT. In the T2DM group, N-terminal propeptide of type 1 collagen (P1NP), a marker of bone formation was 25% lower ($p = 0.013$) and C-terminal telopeptide of type 1 collagen (CTx), a marker of bone resorption was 31% lower ($p = 0.043$) compared to the NGT group. Additionally, P1NP was 24% lower ($p = 0.014$) in the T2DM group compared to the IGT group. No differences were found among the groups in the levels of 25-hyrdoxyvitamin D, creatinine, calcium, phosphorous, estimated glomerular filtration rate (eGFR), sclerostin or pentosidine.

2.3.2 Nanoindentation

In cortical bone, the T2DM group had a higher indentation modulus and hardness compared to the NGT group (indentation modulus +9%, $p = 0.021$; hardness +8%, $p = 0.039$) (Supplementary Table 2.1, Figure 2.2B, 2.2D). Further, when material properties were analyzed within sub-regions of the cortex, T2DM interstitial bone was stiffer and trended toward being harder than osteonal bone (indentation modulus +4%, $p = 0.005$; hardness +2%, $p = 0.071$) (Figure 2.2A, 2.2C). This trend was seen only in the T2DM group but not in the NGT group. Additionally, the osteonal tissue had similar material properties between the groups.

In trabecular bone, indentation modulus and hardness did not differ with study group (Supplementary Table 2.1, Figure 2.3B, 2.3D). The center of the trabecula was stiffer and harder compared to tissue at the formation label and the edge (indentation modulus: +22% vs. label, +8% vs. edge; hardness: +10% vs. label, +6% vs. edge; all $p < 0.001$). Further, the edge of the trabecula was stiffer and trended toward being harder compared to tissue at the formation label (indentation modulus +12%, $p < 0.001$; hardness +3%, $p = 0.076$) (Figure 2.3A, 2.3C). These

trends in sub-region material properties persisted in both NGT and T2DM groups except the comparisons between label and edge sub-regions did not reach statistical significance (Supplementary Table 2.2).

Table 2.3. Participant characteristics by group. Values shown are mean ± standard deviation unless otherwise noted. Statistical significance determined by Kruskal-Wallis H test or Chi-square test at a significance level of 0.05. Abbreviations: NGT = normal glucose tolerance group; IGT = impaired glucose tolerance group; T2DM = type 2 diabetes mellitus group; OGTT = oral glucose tolerance test; eGFR = estimated glomerular filtration rate; CTx = carboxy-terminal telopeptide of type 1 collagen; P1NP = amino-terminal propeptide of type 1 collagen; ucOC = undercarboxylated osteocalcin; n/a = not applicable. Adapted from [38].

Characteristics	**NGT**	**IGT**	**T2DM**	**NGT vs. IGT**	**NGT vs. T2DM**	**IGT vs. T2DM**	**Chi Square Tests of Independence**
n	35	26	23				
Anthropometric							
Age (years)	64.8 ± 6.8	64.4 ± 5.4	63.8 ± 6.2				
Weight (kg)	76.4 ± 14.6	94.0 ± 22.9	94.3 ± 16.4	p = 0.0033	p = 0.0009		
Height (cm)	160.8 ± 6.7	165.6 ± 6.5	160.9 ± 5.9	p = 0.022		p = 0.058	
BMI (kg/m^2)	29.6 ± 5.6	34.3 ± 8.4	36.5 ± 6.9	p = 0.0187	p = 0.00072		
Race/ethnicity							χ^2 (6) = 19.883; p = 0.002905
White, n (%)	27 (77)	13 (50)	6 (24)				

Black, n (%)	8 (23)	11 (42)	17 (68)				
Asian, n (%)	0 (0)	1 (4)	0 (0)				
Hispanic, n (%)	0 (0)	0 (0)	0 (0)				
Other, n (%)	0 (0)	1 (4)	2 (8)				
Bone Densititometry, DXA							
Lumbar Spine (g/cm^2)	1.18 (0.17)	1.28 (0.23)	1.28 (0.19)				
Total Hip (g/cm^2)	0.99 (0.13)	1.03 (0.13)	1.09 (0.14)				
Femoral Neck (g/cm^2)	0.93 (0.10)	0.94 (0.12)	1.00 (0.14)				
T2DM Status at Baseline Visit							
T2DM dx duration (years)	n/a	n/a	14.5 ± 8.4	*n/a*	*n/a*	*n/a*	
OGTT (mg/dL)	95.5 ± 18.2	163.5 ± 29.8	*n/a*	<< 0.0001	*n/a*	*n/a*	
HbA1c (%)	5.8 ± 0.3	6.0 ± 0.4	9.1 ± 2.2		0.008	<< 0.0001	
T2DM-related Drugs							
Insulin, n (%)	0 (0)	0 (0)	25 (100)				$\chi 2$ (2) = 86; p << 0.001
Insulin duration (years)	0 (0)	0 (0)	9.3 (8.4)	*n/a*	*n/a*	*n/a*	
Metformin, n (%)	0 (0)	0 (0)	14 (56)				$\chi 2$ (2) = 40.802; p << 0.001
Sulfonylurea, n (%)	0 (0)	0 (0)	2 (8)				

Other Supplements							
Calcium, n (%)	8 (23)	6 (23)	3 (12)				
Vitamin D, n (%)	13 (37)	11 (42)	11 (44)				
Multi-vitamin, n (%)	15 (43)	10 (38)	4 (16)				
Statin, n (%)	8 (23)	9 (35)	12 (48)				
Acetylsalicylic acid (aspirin), n (%)	15 (43)	7 (27)	12 (48)				
Serum and Urinary Parameters							
25-hydroxyvitamin D (ng/mL)	33.46 ± 9.41	33.23 ± 10.11	30.64 ± 7.31				
Creatinine (mg/dL)	0.81 ± 0.16	0.87 ± 0.20	0.84 ± 0.16				
Calcium (mg/dL)	9.44 ± 0.30	9.51 ± 0.42	9.44 ± 0.39				
Phosphorous (mg/dL)	3.65 ± 0.49	3.48 ± 0.51	3.57 ± 0.66				
Alkaline phosphatase (U/L)	73.57 ± 17.95	72.96 ± 19.84	88.08 ± 24.09		p = 0.041	p = 0.055	
Parathyroid Hormone (pg/mL)	28.77 ± 13.00	39.93 ± 17.59	33.48 ± 16.66	p = 0.028			
eGFR (mL/min/1.73 m^2)	80.49 ± 16.29	80.81 ± 13.46	80.08 ± 15.99				
P1NP (ng/mL)	58.78 ± 23.65	57.83 ± 18.62	44.20 ± 14.07		p = 0.014	p = 0.013	
CTx (ng/mL)	0.32 ± 0.18	0.31 ± 0.22	0.22 ± 0.11		p = 0.043		

Sclerostin (pmol/L)	238.34 ± 98.96	224.50 ± 68.44	229.95 ± 101.36				
ucOC (ng/mL)	3.53 ± 2.00	3.15 ± 2.13	2.66 ± 2.37		p = 0.027		
Pentosidine (nmol/L)	56.25 ± 15.94	51.49 ± 13.54	53.89 ± 13.80				

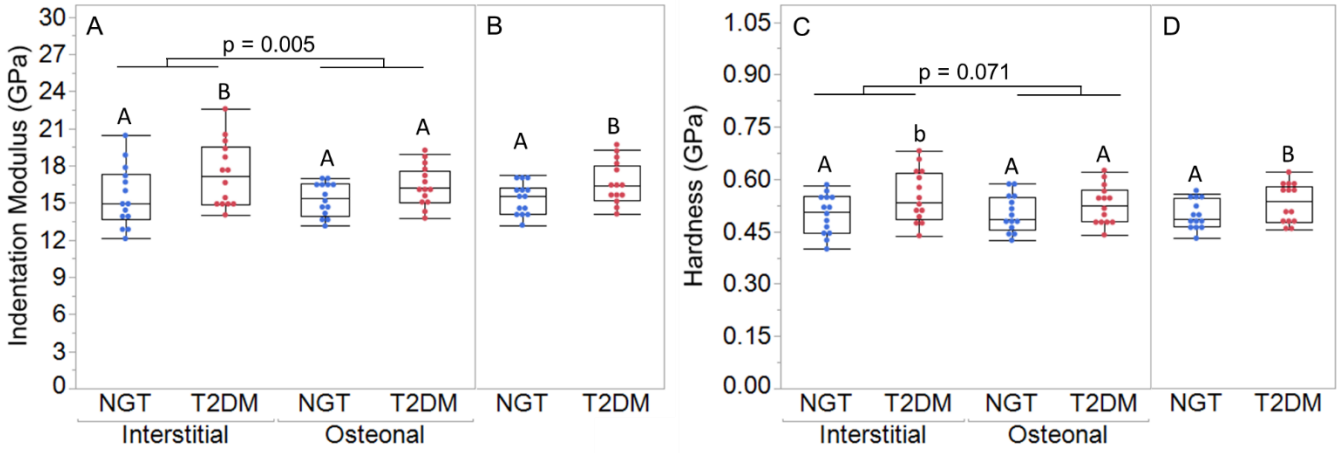

Figure 2.2. Box plots of nanoindentation outcomes in cortical bone plotted by study group and tissue sub-region: (A) indentation modulus and (C) hardness . Each overlaid jittered point represents the average value of 8 interstitial or 30 osteonal measurements per specimen. Specimen-average values (38 measurements per sample) of cortical (B) indentation modulus and (D) hardness by study group. Uppercase letters represent $p < 0.05$ and lowercase letters represent $p < 0.10$. Abbreviations: NGT = Normal glucose tolerance; T2DM = Type 2 diabetes mellitus.

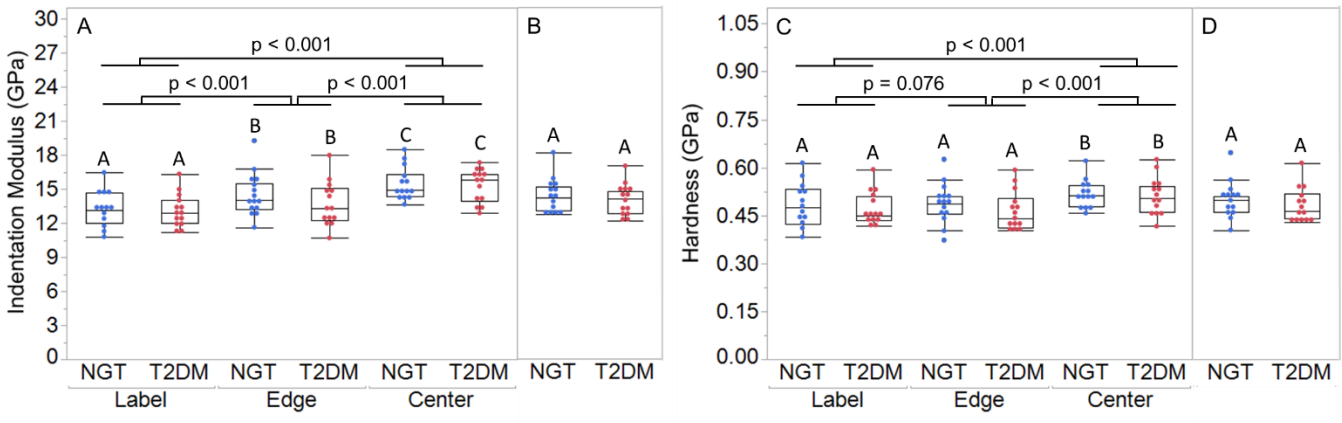

Figure 2.3. Box plots of nanoindentation outcomes in trabecular bone plotted by study group and tissue sub-region: (A) indentation modulus and (C) hardness . Each overlaid jittered point represents the average value of 10 measurements in either label or edge or center sub-regions per specimen. Specimen-average values (30 measurements per sample) of trabecular (B) indentation modulus and (D) hardness by study group. Uppercase letters represent $p < 0.05$ and lowercase letters represent $p < 0.10$. Abbreviations: NGT = Normal glucose tolerance; T2DM = Type 2

diabetes mellitus.

Supplementary Table 2.1. Nanoindentation outcomes in NGT and T2DM groups in cortical and trabecular bone stratified by tissue sub-region.

Parameter	NGT	T2DM	% difference vs. NGT	p-value (NGT vs. T2DM)
Indentation Modulus (GPa)				
Cortical bone	15.4 ± 1.54	16.8 ± 1.54	9	**0.021**
Osteonal bone	15.2 ± 1.54	16.3 ± 1.54	7	0.252
Interstitial bone	15.5 ± 1.75	17.3 ± 1.75	12	**0.008**
Trabecular bone	14.3 ± 1.42	13.9 ± 1.42	-3	0.468
Label	12.9 ± 1.60	12.4 ± 1.57	-4	0.959
Edge	14.4 ± 1.50	14.0 ± 1.51	-3	0.958
Center	15.5 ± 1.54	15.3 ± 1.54	-1	0.999
Hardness (GPa)				
Cortical bone	0.50 ± 0.05	0.54 ± 0.05	8	**0.039**
Osteonal bone	0.50 ± 0.05	0.53 ± 0.05	6	0.434
Interstitial bone	0.50 ± 0.06	0.55 ± 0.06	11	0.062
Trabecular bone	0.49 ± 0.05	0.48 ± 0.05	-3	0.498
Label	0.48 ± 0.06	0.46 ± 0.06	-4	0.971
Edge	0.49 ± 0.05	0.48 ± 0.06	-2	0.981
Center	0.52 ± 0.05	0.51 ± 0.06	-2	0.998

Supplementary Table 2.2. Nanoindentation outcomes in cortical and trabecular tissue subregions stratified by study group.

Parameter	Cortical Bone		% differences (interstitial vs. osteonal)	p-values (interstitial vs. osteonal)	Trabecular Bone			% differences			p-values		
	Osteonal	Interstitial			Label	Edge	Center	center vs. label	center vs. edge	edge vs. label	center vs. label	center vs. edge	edge vs. label
Indentation Modulus (GPa)													
NGT	15.2 ± 1.54	15.5 ± 1.75	2	0.840	12.9 ± 1.60	14.4 ± 1.50	15.5 ± 1.54	20	8	12	**<0.001**	**0.001**	**<0.001**
T2DM	16.3 ± 1.54	17.3 ± 1.75	6	**0.008**	12.4 ± 1.57	14.0 ± 1.51	15.3 ± 1.54	24	9	13	**<0.001**	**<0.001**	**<0.001**
Hardness (GPa)													
NGT	0.50 ± 0.05	0.50 ± 0.06	0	1.000	0.48 ± 0.06	0.49 ± 0.05	0.52 ± 0.05	8	6	2	**0.002**	**0.030**	0.866
T2DM	0.53 ± 0.05	0.55 ± 0.06	4	0.056	0.46 ± 0.06	0.48 ± 0.06	0.51 ± 0.06	11	6	4	**<0.001**	**<0.001**	0.941

2.3.3 Raman Spectroscopy

In cortical bone, none of the Raman compositional parameters were different with study group. Across NGT and T2DM groups, composition varied across osteonal and interstitial sub-regions. Specifically, interstitial bone had higher mineral:matrix ratio and mineral maturity/crystallinity compared to osteonal bone (M:M +7%, $p < 0.001$; XST +1%, $p < 0.001$) (Figure 2.4A, 2.4B). No differences were observed in carbonate:phosphate ratio with tissue sub-region (Figure 2.4C). Additionally, in the T2DM group only, the interstitial bone had higher pyridinoline content (+6%, $p < 0.001$). Glycosaminoglycan content trended to be lower in interstitial bone compared to the osteonal bone; (GAG -4%, $p = 0.077$) (Figure 2.4D, Supplementary Figure 2.2A).

In trabecular bone, none of the Raman compositional parameters were different with study group, Across NGT and T2DM groups, composition varied within trabecular sub-regions. Specifically, the center of the trabecula had greater mineral:matrix ratio, mineral maturity/crystallinity, and carbonate:phosphate ratio compared to the edge (M:M +6%, $p < 0.001$; XST +0.4%, $p = 0.072$; C:P +15%, $p < 0.001$) (Figure 2.5A, 2.5B, 2.5C). Further, tissue at the center and the edge of the trabeculae had higher carbonate:phosphate ratio compared to that at the fluorochrome label (+21% vs. center, $p < 0.001$; +5% vs. edge, $p = 0.052$). The trends in mineral content were seen only in the T2DM group but not in the NGT group. The trends in crystallinity persisted in both NGT and T2DM groups except the comparisons between edge and maker sub-regions which were not significant. The center of the trabecula had higher pyridinoline content compared to the edge (+8%, $p = 0.002$) and label (+12%, $p < 0.001$) sub-regions (Figure 2.5D). Additionally, the edge of the trabecula had lower GAG content compared

to the label (-7%, p = 0.075) (Supplementary Figure 2.2B). The GAG content was higher in the center of the trabecula compared to the edge (+8%, p = 0.042).

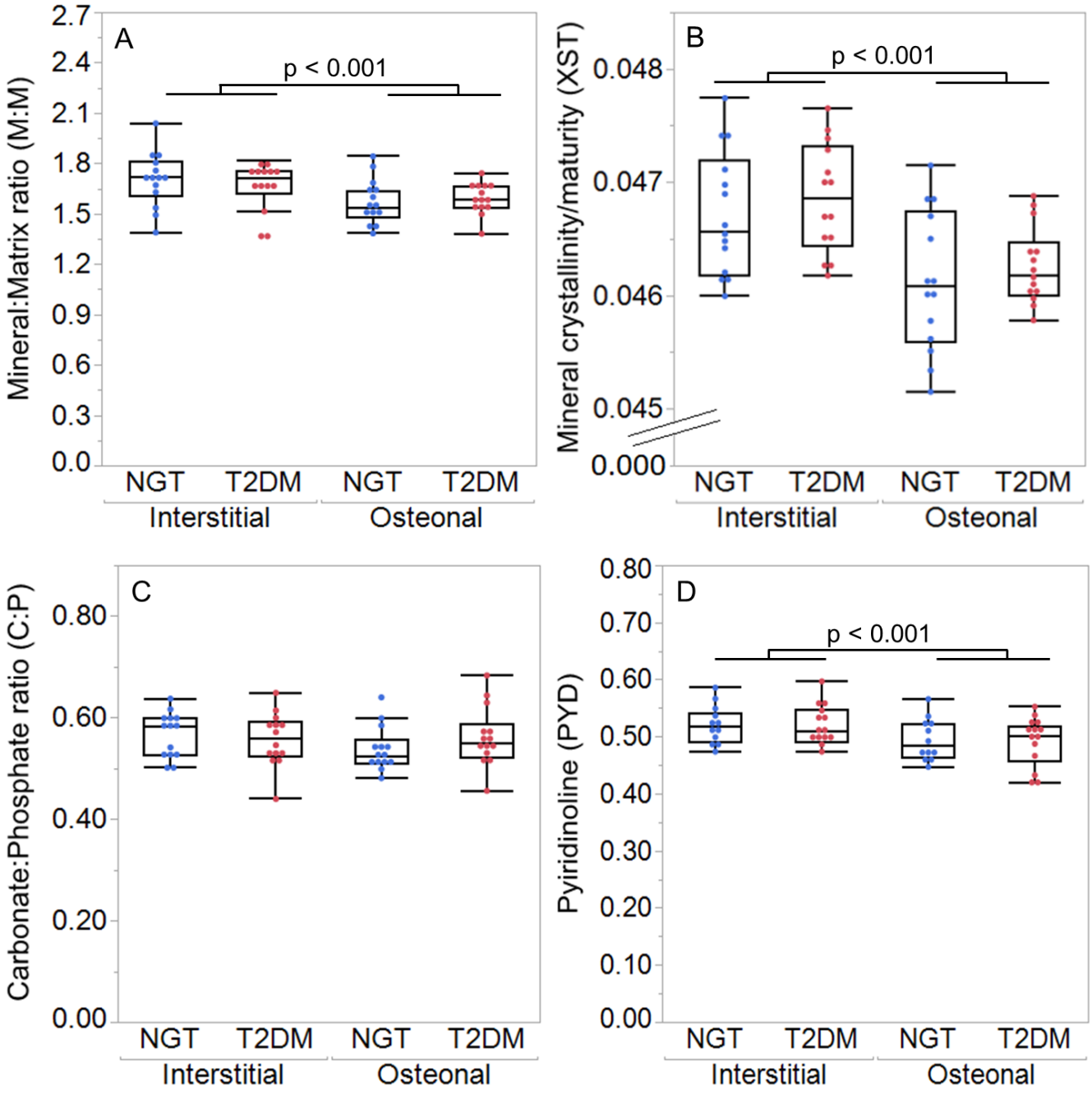

Figure 2.4. Box plots of Raman spectroscopic outcomes in cortical bone plotted by study group and tissue sub-region: (A) Mineral:Matrix ratio (M:M), (B) Mineral crystallinity / maturity (XST), (C) Carbonate:Phosphate ratio (C:P), (D) Pyridinoline (PYD) content. Each overlaid

jittered point represents the average value from the 9 spectra collected in each sub-region per specimen. Abbreviations: NGT = Normal glucose tolerance; T2DM = Type 2 diabetes mellitus.

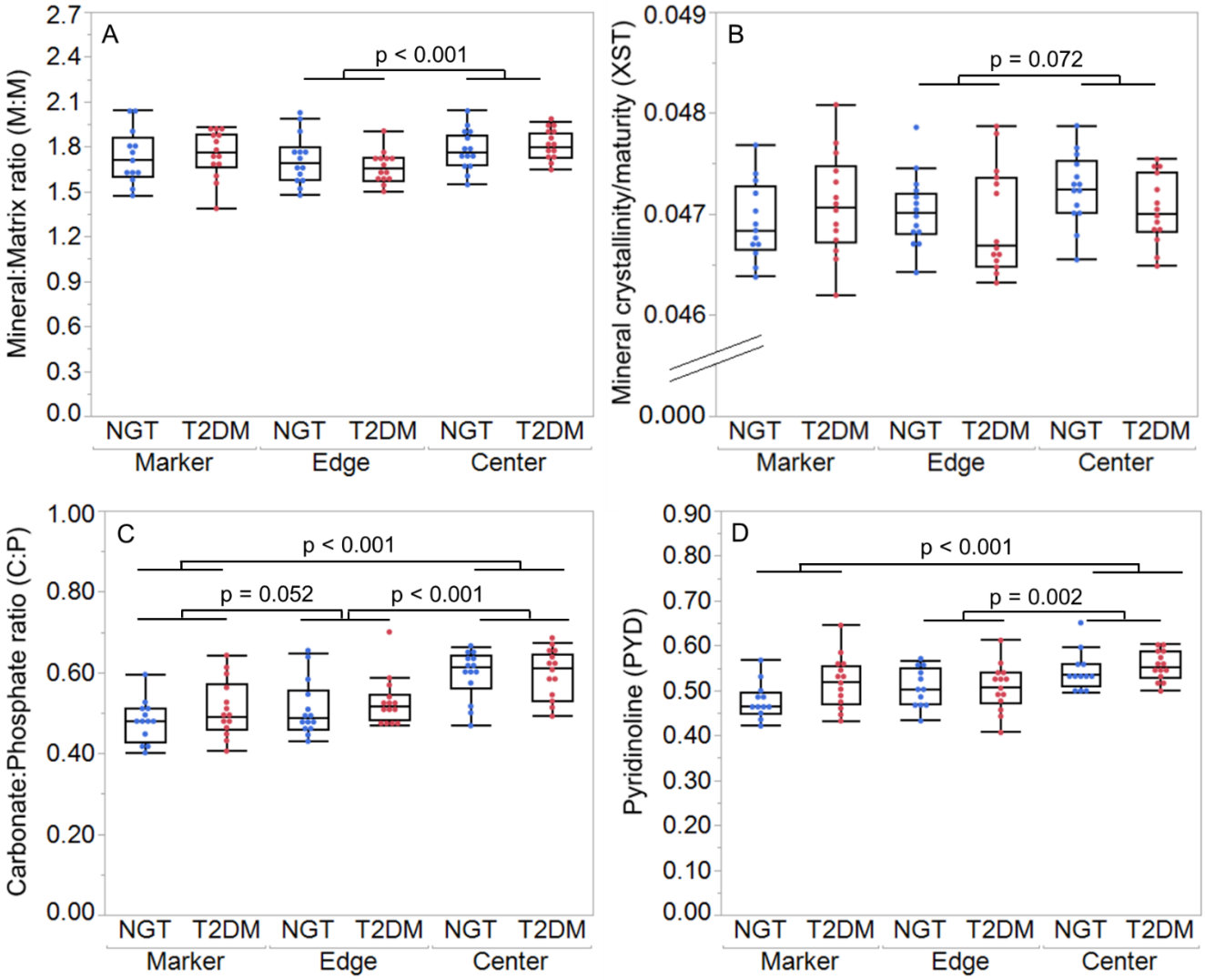

Figure 2.5. Box plots of Raman spectroscopic outcomes in trabecular bone plotted by study group and tissue sub-region: (A) Mineral:Matrix ratio (M:M), (B) Mineral crystallinity / maturity (XST), (C) Carbonate:Phosphate ratio (C:P), (D) Pyridinoline (PYD) content. Each overlaid jittered point represents the average value from the 9 spectra collected in each sub-region per specimen. Abbreviations: NGT = Normal glucose tolerance; T2DM = Type 2 diabetes mellitus.

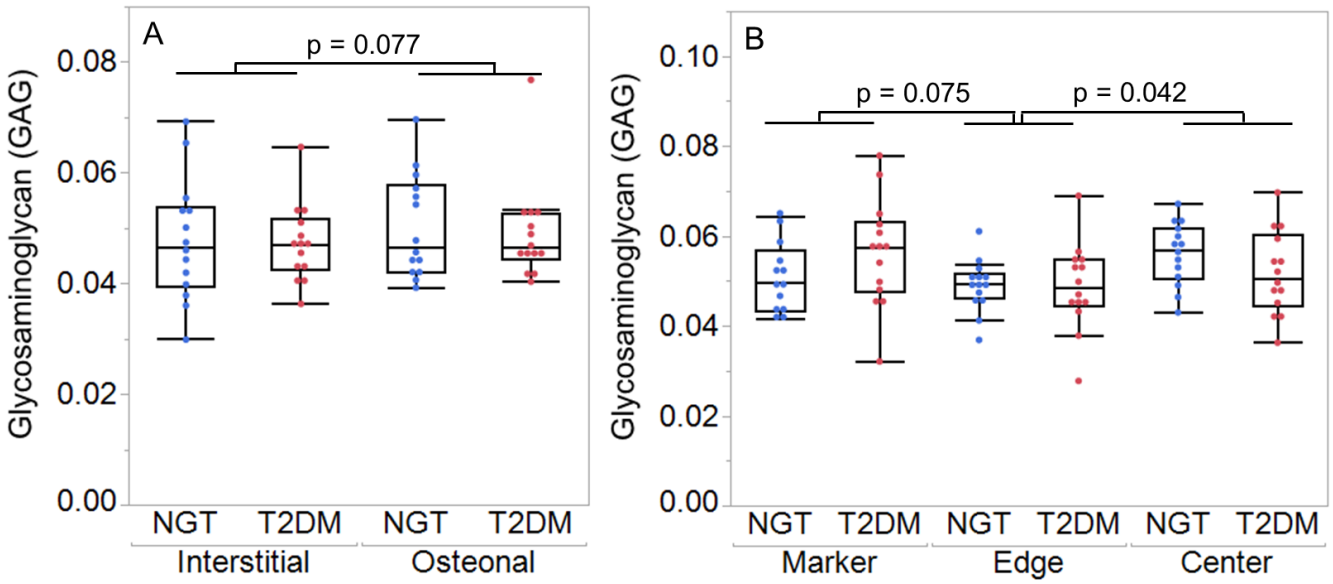

Supplementary Figure 2.2. Box plots of glycosaminoglycan content in (A) cortical bone and (B) trabecular bone plotted by study group and tissue sub-region. Each overlaid jittered point represents the average value from the 9 spectra collected in each sub-region per specimen. Abbreviations: NGT = Normal glucose tolerance; T2DM = Type 2 diabetes mellitus.

2.3.4 Confocal/Multiphoton Imaging

Bone from the T2DM group had a greater mean normalized fluorescent AGE content compared to that from the NGT group (cortical +77%, $p < 0.001$; trabecular +57%, $p < 0.001$) (Figure 2.6, 7A, 8A). Qualitatively, the relatively older tissue (interstitial bone in the cortical region and the center of the trabeculae) had higher fAGE content compared to the younger tissue (Figure 2.6).

Further, bone from the T2DM group had more variable fAGE content, as evidenced by the greater standard deviation of fluorescence intensity compared to that from the NGT group (cortical +54%, $p < 0.001$; trabecular +32%, $p < 0.001$) (Figure 2.7B, 2.8B).

First and second order statistical parameters of collagen organization in both cortical and trabecular bone were not different between T2DM and NGT groups (data not shown).

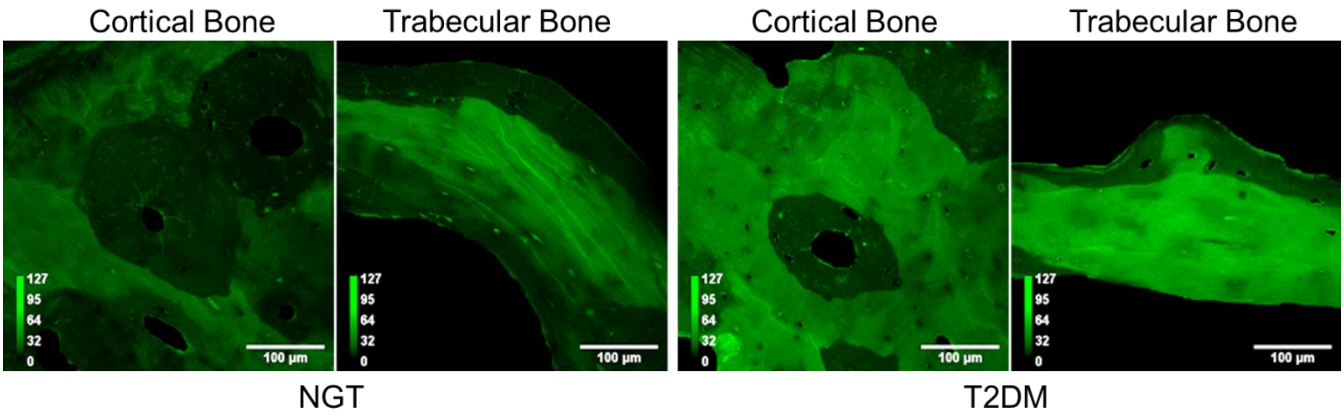

Figure 2.6. Representative false color fluorescent AGE images of cortical and trabecular bone from NGT (left) and T2DM (right) groups. Color image scale represents fAGE intensity normalized by fluorescence from C-687 dye. Scale bar – 100 µm

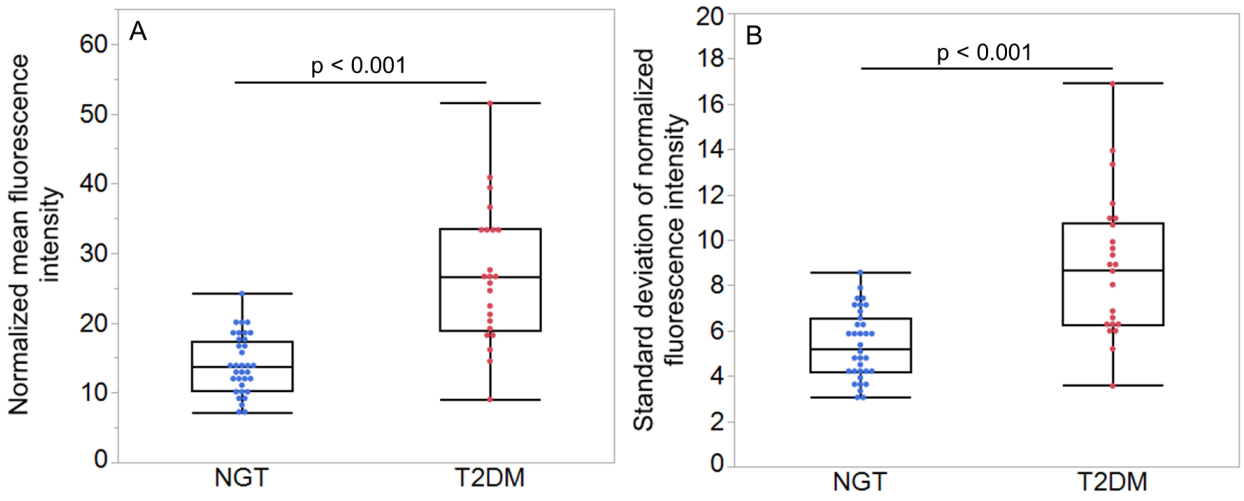

Figure 2.7. Box plots of cortical bone (A) mean of normalized fluorescence intensity distribution, (B) standard deviation of normalized fluorescence intensity distribution, plotted as a function of study group. Each overlaid jittered point represents mean of the parameter from all three cortical regions of interest per sample. Abbreviations: NGT = Normal glucose tolerance; T2DM = Type 2 diabetes mellitus.

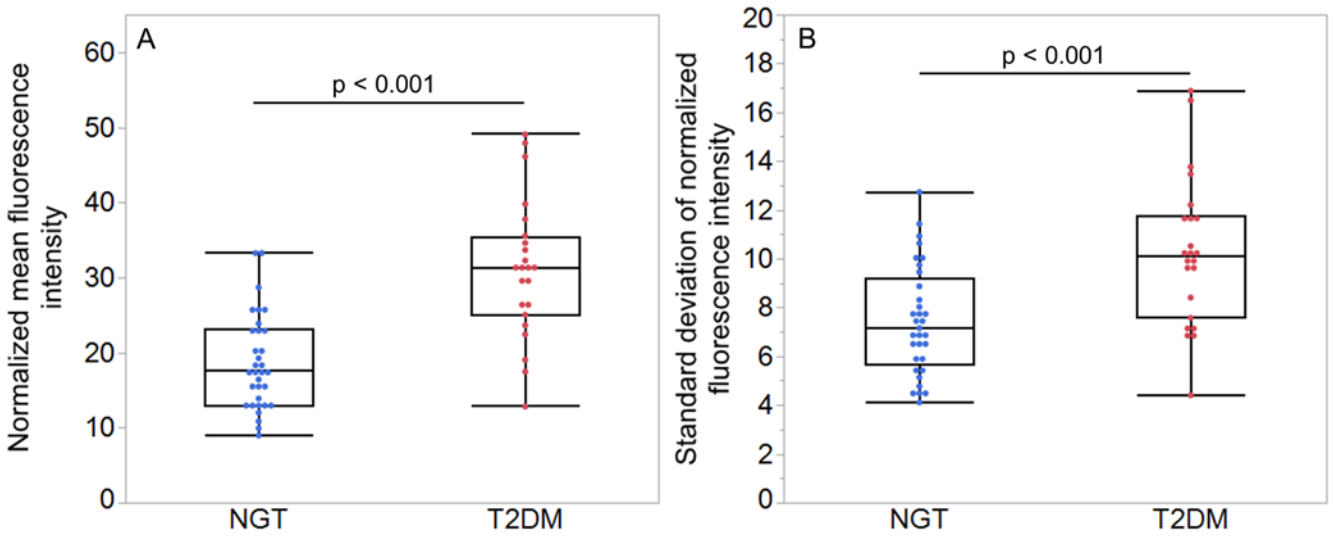

Figure 2.8. Box plots of trabecular bone (A) mean of normalized fluorescence intensity distribution, (B) standard deviation of normalized fluorescence intensity distribution, plotted as a function of study group. Each overlaid jittered point represents mean of the parameter from all three trabecular regions of interest per sample. Abbreviations: NGT = Normal glucose tolerance; T2DM = Type 2 diabetes mellitus.

2.3.5 Analysis of relationships between glycemic control, compositional properties and mechanical properties

When compositional properties were examined as a function of glycemic control, normalized mean fluorescent AGE content of cortical and trabecular bone increased with HbA1c (Cortical: R2 = 0.36, $p < 0.001$; Trabecular: R2 = 0.33, $p < 0.001$; Pooled: $R^2 = 0.33$, $p < 0.001$) (Figure 2.9). The relationships for cortical and trabecular bone were similar: the slopes of the cortical and trabecular regression lines were not different. These relationships were not significant when separate regression lines were made for the NGT and the T2DM groups. Mechanical or compositional properties of cortical or trabecular bone did not correlate with HbA1c.

When relationships between mechanical and compositional properties were examined, regression modeling adjusted for repeated measures showed that Raman mineral crystallinity /

maturity and glycosaminoglycan content positively correlated with indentation modulus (XST: p = 0.005; GAG: p = 0.090) and only glycosaminoglycan content positively correlated with hardness (GAG: p = 0.018) (Table 2.4). Finally, no relationships were observed between mechanical properties assessed by nanoindentation and fluorescent AGE content.

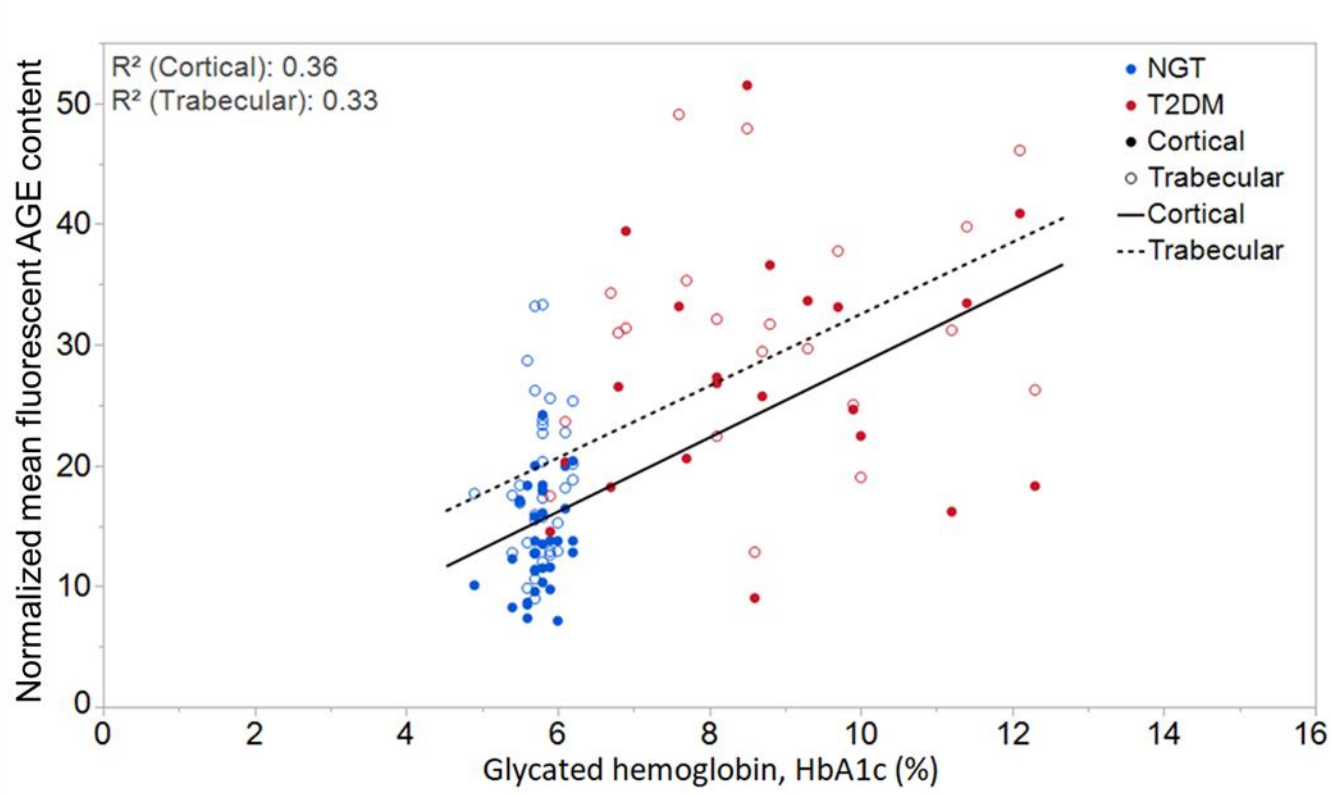

Figure 2.9. Relationship between cortical and trabecular mean fluorescent AGE content and HbA1c. Solid black lines indicate the regression fit for the cortical bone, and dotted black line indicate the regression fit for the trabecular bone. Each open or closed circle indicates the mean of fluorescent AGE content from all three cortical or three trabecular regions of interest per sample.

Table 2.4. Regression modelling of mechanical and compositional properties. Values are shown as parameter coefficients with standard error in parentheses.

Parameter	**Modulus**	**p-value**	**Hardness**	**p-value**
Intercept	-33.6 (15.1)	0.029	-0.4 (0.4)	0.367
Mineral:Matrix ratio	-0.8 (1.5)	0.612	-0.004 (0.04)	0.929

Mineral crystallinity / maturity	1006.0 (348.5)	**0.005**	16.4 (10.4)	0.118
Carbonate:Phosphate ratio	2.1 (3.8)	0.588	0.08 (0.1)	0.470
Glycosaminoglycan	36.5 (21.3)	0.090	1.5 (0.6)	**0.018**
Pyridinoline	2.3 (3.7)	0.542	0.1 (0.1)	0.360

2.4 Discussion

In this study, we measured nanomechanical and compositional properties of iliac cortical and trabecular bone from postmenopausal women with normal glucose tolerance and overt type 2 diabetes. As hypothesized, women with overt T2DM had higher cortical and trabecular AGE content compared to women with NGT, and the AGE content increased with HbA1c. Further, the cortical tissue from individuals with T2DM was stiffer and harder compared to that in individuals with NGT.

The T2DM group had reduced bone remodeling compared to the NGT group, as indicated by the serum markers of bone turnover. Specifically, the serum P1NP content, a marker of bone formation, and CTx content, a marker of bone resorption, were lower in the T2DM group compared to the NGT group and P1NP was also lower in the T2DM group compared to the IGT group but did not differ otherwise. These results indicate that bone formation is reduced during the transition from pre-diabetes to T2DM but remains unaltered during pre-diabetes. However, bone resorption is reduced during the transition from NGT through T2DM. This loss in resorption before reduction in formation may explain the preserved or increased BMD in individuals with T2DM. Overall, these results are in accordance with prior histomorphometric and serum studies demonstrating that individuals with T2DM have reduced bone remodeling compared to non-diabetic individuals.[13–15,54]

As hypothesized, both cortical and trabecular bone from the T2DM group had higher fluorescent AGE content compared to the NGT group. Similarly, pentosidine, a crosslinking AGE, assessed by HPLC was higher in cortical and trabecular bone in men with T2DM compared to non-DM men;[25,27] however, total fluorescent AGE content measured by a fluorometric assay was only higher in cortical bone but not in trabecular bone.[25,26] We observed higher AGEs in both cortical and trabecular bone with T2DM and the AGE content was higher in cortical bone compared to trabecular bone. Higher turnover in trabecular bone resulting in remodeling of bone tissue with higher AGEs may explain lower AGEs in trabecular bone compared to cortical bone. The differences observed in AGEs with study group may have been more pronounced in the current study than those observed in prior work because our T2DM population had relatively poor glycemic control [HbA1c = 9.1 ± 2.2 vs. 7.1 ± 0.9[25], 7.0 ± 1.3[26]].

Additionally, quantitative multiphoton images of AGE concentration provided spatially resolved maps of AGE accumulation for the first time, to our knowledge, in a T2DM population. This analysis demonstrated that the relatively older tissue (interstitial bone in the cortical region and the center of the trabecula) had higher fAGE content compared to the younger tissue in both NGT and T2DM groups. These results indicate that AGEs accumulate in the less remodeled regions of the bone. Furthermore, AGEs accumulate in the less remodeled regions as evidenced by the higher AGEs in the relatively older sub-regions in the T2DM group compared to the NGT group where the differences are faint between the tissue sub-regions (Figure 2.6). The large variation in AGE concentration within images in the T2DM group was reflected in the greater standard deviation of fluorescence intensity compared to the NGT group.

Second harmonic generation images of collagen were obtained to study the effects of the altered crosslinking profile on the microscale structure of collagen. No differences were observed in the collagen content and organization in cortical or trabecular bone with study group. This result indicates that the biochemical changes in the type of crosslinking does not affect the microstructural organization of collagen.

The nanomechanical properties of cortical bone were altered but of the trabecular bone were preserved in the T2DM group compared to the NGT group. The T2DM group had stiffer and harder cortices compared to the NGT group . In cortical bone, only the interstitial tissue was stiffer and trended towards higher hardness in the T2DM group compared to that in the NGT group. The relatively newer tissue, the osteonal tissue, had similar material properties between the groups. Additionally, when the NGT and T2DM group data was pooled, interstitial sub-region was stiffer and harder compared to the osteonal sub-regions consistent with previous studies.[55–57] But this variation was observed only in the T2DM group but not in the NGT group. The trabecular bone mechanical properties were not different between the groups but showed consistent trends by sub-region, consistent with previous studies[58]: the central region was hardest and stiffest; the edge had intermediate values; and the label region was softest and most compliant. Overall, these results indicate that the cortex had more profound changes in material properties than cancellous tissue, potentially due to slower remodeling in cortical bone.

In both cortical and trabecular bone, Raman compositional outcomes did not differ with study group but were consistent with relative tissue age. Previous Fourier transform infrared (FTIR) and quantitative backscattered electron imaging studies reported higher mineralization in trabecular bone from individuals with T2DM vs. non-DM individuals.[25,32] Additionally, FTIR characterization on the full cohort from this study showed that the T2DM group had higher

cortical mineral content compared to that of the NGT group.[38] But surprisingly, none of these previously reported differences in bone composition with T2DM were seen in the current study. Smaller sample size in this study and the differences in Raman and FTIR vibrational techniques may be responsible for no differences observed.

The trends in the compositional outcomes with sub-region are generally consistent with the expected properties of recently formed vs. older tissue and agree well with previous studies.[59–61] In contrast, in trabecular bone, the label sub-region had similar mineral content and crystallinity to center and edge sub-regions. This discrepancy can be attributed to the potential interference of demeclocycline in Raman spectra collected from the label sub-region because the fluorophore binds to the mineral. Additionally, the glycosaminoglycan content did not follow a specific trend with tissue age. Although GAG content was higher at the center of the trabecula, consistent with the results in prior studies,[60,61] the relatively younger osteonal and label sub-regions also had higher GAG content compared to the interstitial and the edge sub-regions. It must be noted that the Raman GAG peak has low signal to noise ratio compared other peaks in Table 2.1 and this outcome is not as extensively validated in bone as others. The relatively older tissue had higher mineral content and crystallinity, and collagen maturity compared to the younger tissue in both cortical and trabecular bone.

When relationships among glycemic control and bone tissue composition were examined, regression analysis revealed that poor glycemic control is associated with accumulation of bone tissue AGEs. But HbA1c or AGE content were not significant explanatory variables for the material properties of the bone indicating that AGEs do not directly affect the stiffness or hardness of the bone. This result is expected as the mineral component predominantly dictates elastic properties, and the collagen crosslinking dictates post-yield properties.[62,63]

Surprisingly, mineral content was not associated with indentation modulus or hardness, but mineral crystallinity / maturity positively correlated with indentation modulus indicating that larger and/or more perfect crystals increase tissue stiffness. Since carbonate substitution, a measure of crystal perfection, was not an explanatory variable for indentation modulus, crystal size may independently affect tissue material properties. Previous studies reported a similar relationship between mineral crystallinity and indentation modulus;[64] but the mechanism through which large crystals increase stiffness is unknown.[65]

Taken together, our work shows that bone from individuals with T2DM has altered composition and material properties. Specifically, we found that the bone tissue AGEs were higher in individuals with T2DM and the AGE content was positively associated with glycemic control of the individual. Although, previous studies reported higher AGEs in individuals with T2DM, did not observe any association with HbA1c potentially due to relatively controlled hyperglycemia.[25,26] The key hypothesis for accumulation of AGEs in bone tissue is poor glycemic control and our study confirmed this hypothesis. Additionally, previous in vivo[35–37] and ex vivo[26] microindentation studies reported lower resistance to indentation in cortical bone of individuals with T2DM compared to non-diabetic individuals. However, it is not known (1) if these trends were observed in trabecular bone (2) if microstructure or composition influenced these outcomes and, (3) if these outcomes are associated with tissue material properties. We characterized tissue material properties of both cortical and trabecular bone and found that cortical tissue in individuals with T2DM was stiffer and harder, but the trabecular bone has similar material properties compared to that form individuals with NGT. Overall, these results provide evidence that bone tissue AGEs increase with worsening glycemic control which may reduce bone ductility and contribute to skeletal fragility in individuals with T2DM.

This study has several key strengths and limitations. The strengths of this study are 1) recruitment of individuals with IGT and overt T2DM to study the effects of increasing disease severity on bone quality; 2) it provides the first spatially resolved quantification of AGEs, mechanical and compositional properties of bone from individuals with T2DM; 3) to our knowledge, this is the first study to report nanomechanical properties at fluorochrome label region in human biopsies. The limitations of this study are 1) the iliac crest is not a clinically relevant fracture site and it is unknown if the changes in bone quality with T2DM are systemic; 2) the IGT group was not characterized with nanoindentation and Raman spectroscopy due to modest differences in NGT vs. T2DM outcomes; 3) double fluorochrome labels could not be resolved in the thick embedded bone which otherwise could have provided more tightly controlled sub-regions of known tissue age; 4) The HPLC and fluorescent plate assay experiments are ongoing and could not be finished due to lab shutdown during COVID-19 pandemic. Nevertheless, this study is the first to provide information on bone material properties at nanoscale and the effect of relative tissue age on spatial distribution of AGEs in individuals with T2DM.

2.5 Conclusion

In this study, we measured nanomechanical and compositional properties, and spatial distribution of AGEs, collagen in bone from postmenopausal women with NGT and T2DM. We found that the individuals with T2DM had stiffer and harder cortical bone compared to the individuals with NGT, but no differences were found in the trabecular bone. Further, the cortical and trabecular bone tissue AGE content in the T2DM group was higher compared to the NGT group. The relatively older tissues (cortical vs. trabecular; interstitial vs. osteonal; center vs. edge) had more profound changes in material properties and AGE accumulation due to T2DM. Overall, this

study is the first to provide spatially resolved quantification of AGEs, mechanical and compositional properties of bone from individuals with T2DM and found significant relationship between glycemic derangement and accumulation of bone tissue AGEs.

2.6 Acknowledgement

We thank Dr. Shefford Baker and Zach Rouse for assistance with nanoindentation and Dr. Rebecca Williams and Johanna M. Dela Cruz for assistance with multiphoton imaging.

Imaging data was acquired through the Cornell University Biotechnology Resource Center, with NIH S10OD018516 funding for the shared Zeiss LSM880 confocal/multiphoton microscope.

This work made use of the Cornell Center for Materials Research Shared Facilities which are supported through the NSF MRSEC program (DMR-1719875).

2.7 References

1. Vestergaard P. Discrepancies in bone mineral density and fracture risk in patients with type 1 and type 2 diabetes - A meta-analysis. Osteoporos Int. 2007;18:427–44.

2. Janghorbani M, Van Dam RM, Willett WC, Hu FB. Systematic review of type 1 and type 2 diabetes mellitus and risk of fracture. Am J Epidemiol. 2007;166:495–505.

3. Schwartz A V., Vittinghoff E, Bauer DC, Hillier TA, Strotmeyer ES, Ensrud KE, et al. Association of BMD and FRAX score with risk of fracture in older adults with type 2 diabetes. JAMA - J Am Med Assoc. 2011;305:2184–92.

4. Bonds DE, Larson JC, Schwartz A V., Strotmeyer ES, Robbins J, Rodriguez BL, et al. Risk of fracture in women with type 2 diabetes: The women's health initiative observational study. J Clin Endocrinol Metab. 2006;91:3404–10.

5. Starup-Linde J, Frost M, Vestergaard P, Abrahamsen B. Epidemiology of Fractures in Diabetes. Calcif Tissue Int. Elsevier Inc.; 2017;100:109–21.

6. Schwartz A V. Epidemiology of fractures in type 2 diabetes. Bone. 2016;82:2–8.

7. De Liefde II, Van Der Klift M, De Laet CEDH, Van Daele PLA, Hofman A, Pols HAP. Bone mineral density and fracture risk in type-2 diabetes mellitus: The Rotterdam Study. Osteoporos Int. Springer; 2005;16:1713–20.

8. Napoli N, Strotmeyer ES, Ensrud KE, Sellmeyer DE, Bauer DC, Hoffman AR, et al. Fracture risk in diabetic elderly men: The MrOS study. Diabetologia. Springer Verlag; 2014;57:2057–65.

9. Strotmeyer ES, Cauley JA, Schwartz A V., Nevitt MC, Resnick HE, Bauer DC, et al. Nontraumatic fracture risk with diabetes mellitus and impaired fasting glucose in older white and black adults: The health, aging, and body composition study. Arch Intern Med. Arch Intern Med; 2005;165:1612–7.

10. Napoli N, Chandran M, Pierroz DD, Abrahamsen B, Schwartz A V., Ferrari SL. Mechanisms of diabetes mellitus-induced bone fragility. Nat Rev Endocrinol. Nature Publishing Group; 2017;13:208–19.

11. Shanbhogue V V., Mitchell DM, Rosen CJ, Bouxsein ML. Type 2 diabetes and the skeleton: New insights into sweet bones. Lancet Diabetes Endocrinol. 2016;4:159–73.

12. Hamann C, Kirschner S, Günther KP, Hofbauer LC. Bone, sweet bone - Osteoporotic fractures in diabetes mellitus. Nat Rev Endocrinol. Nature Publishing Group; 2012;8:297–305.

13. Manavalan JS, Cremers S, Dempster DW, Zhou H, Dworakowski E, Kode A, et al. Circulating Osteogenic Precursor Cells in Type 2 Diabetes Mellitus. J Clin Endocrinol Metab. 2012;97:3240–50.

14. Krakauer JC, McKenna MJ, Buderer NF, Rao DS, Whitehouse FW, Parfitt AM. Bone loss and bone turnover in diabetes. Diabetes. American Diabetes Association; 1995;44:775–82.

15. Hygum K, Starup-Linde J, Harsløf T, Vestergaard P, Langdahl BL. Diabetes mellitus, a state of low bone turnover-a systematic review and meta-analysis. Eur J Endocrinol. 2017;176:R137–57.

16. Starup-Linde J, Vestergaard P. Biochemical bone turnover markers in diabetes mellitus - A systematic review. Bone. Elsevier Inc.; 2016;82:69–78.

17. Costantini S, Conte C. Bone health in diabetes and prediabetes. World J Diabetes. Baishideng Publishing Group Inc.; 2019;10:421–45.

18. Tai K, Dao M, Suresh S, Palazoglu A, Ortiz C. Nanoscale heterogeneity promotes energy dissipation in bone. Nat Mater. 2007;6:454–62.

19. Seref-Ferlengez Z, Kennedy OD, Schaffler MB. Bone microdamage, remodeling and bone fragility: how much damage is too much damage? Bonekey Rep. Portico; 2015;4:644.

20. Koester KJ, Ager JW, Ritchie RO. The true toughness of human cortical bone measured with realistically short cracks. Nat Mater. Nature Publishing Group; 2008;7:672–7.

21. Zimmermann EA, Ritchie RO. Bone as a Structural Material. Adv Healthc Mater. Wiley-VCH Verlag; 2015;4:1287–304.

22. Sassi F, Buondonno I, Luppi C, Spertino E, Stratta E, Di Stefano M, et al. Type 2 diabetes affects bone cells precursors and bone turnover. BMC Endocr Disord. BioMed Central Ltd.; 2018;18.

23. Hu Z, Ma C, Liang Y, Zou S, Liu X. Osteoclasts in bone regeneration under type 2 diabetes mellitus. Acta Biomater. Acta Materialia Inc; 2019;84:402–13.

24. Taylor EA, Donnelly E. Raman and Fourier transform infrared imaging for characterization of bone material properties. Bone. Elsevier BV; 2020;139:115490.

25. Hunt HB, Torres AM, Palomino PM, Marty E, Saiyed R, Cohn M, et al. Altered Tissue Composition, Microarchitecture, and Mechanical Performance in Cancellous Bone From Men With Type 2 Diabetes Mellitus. J Bone Miner Res. 2019;34:1191–206.

26. Karim L, Moulton J, Van Vliet M, Velie K, Robbins A, Malekipour F, et al. Bone microarchitecture, biomechanical properties, and advanced glycation end-products in the proximal femur of adults with type 2 diabetes. Bone. Elsevier; 2018;114:32–9.

27. Bucknell A, King KB, Oren TW, Botolin S, Williams A. Arthroplasty in veterans: Analysis of cartilage, bone, serum, and synovial fluid reveals differences and similarities in osteoarthritis with and without comorbid diabetes. J Rehabil Res Dev. 2012;48:1195.

28. Karim L, Tang SY, Sroga GE, Vashishth D. Differences in non-enzymatic glycation and collagen cross-links between human cortical and cancellous bone. Osteoporos Int. 2013;24:2441–7.

29. Kida Y, Saito M, Shinohara A, Soshi S, Marumo K. Non-invasive skin autofluorescence, blood and urine assays of the advanced glycation end product (AGE) pentosidine as an indirect

indicator of AGE content in human bone. BMC Musculoskelet Disord. BioMed Central Ltd.; 2019;20:1–8.

30. Saito M, Fujii K, Mori Y, Marumo K. Role of collagen enzymatic and glycation induced cross-links as a determinant of bone quality in spontaneously diabetic WBN/Kob rats. Osteoporos Int. 2006;17:1514–23.

31. Saito M, Marumo K. Collagen Cross-Links as a Determinant of Bone Quality. Skelet Adapt to Mech Strain A Key Role Osteoporos. Springer Japan; 2015. p. 35–54.

32. Pritchard JM, Papaioannou A, Tomowich C, Giangregorio LM, Atkinson SA, Beattie KA, et al. Bone mineralization is elevated and less heterogeneous in adults with type 2 diabetes and osteoarthritis compared to controls with osteoarthritis alone. Bone. Elsevier Inc.; 2013;54:76–82.

33. Ionova-Martin SS, Wade JM, Tang S, Shahnazari M, Ager JW, Lane NE, et al. Changes in cortical bone response to high-fat diet from adolescence to adulthood in mice. Osteoporos Int. 2011;22:2283–93.

34. Lekkala S, Taylor EA, Hunt HB, Donnelly E. Effects of Diabetes on Bone Material Properties. Curr Osteoporos Rep. 2019;17:455–64.

35. Farr JN, Drake MT, Amin S, Melton LJ, McCready LK, Khosla S. In vivo assessment of bone quality in postmenopausal women with type 2 diabetes. J Bone Miner Res. 2014;29:787–95.

36. Furst JR, Bandeira LC, Fan WW, Agarwal S, Nishiyama KK, Mcmahon DJ, et al. Advanced glycation endproducts and bone material strength in type 2 diabetes. J Clin Endocrinol Metab. 2016;101:2502–10.

37. Nilsson AG, Sundh D, Johansson L, Nilsson M, Mellström D, Rudäng R, et al. Type 2 Diabetes Mellitus Is Associated With Better Bone Microarchitecture But Lower Bone Material Strength and Poorer Physical Function in Elderly Women: A Population-Based Study. J Bone Miner Res. 2017;32:1062–71.

38. Hunt HB. CHARACTERIZATION OF MATERIAL PROPERTIES, MICROARCHITECTURE, AND MECHANICS OF BONE FROM SUBJECTS WITH TYPE 2 DIABETES MELLITUS. 2018.

39. Donnelly E, Baker SP, Boskey AL, Van Der Meulen MCH. Effects of surface roughness and maximum load on the mechanical properties of cancellous bone measured by nanoindentation. J Biomed Mater Res - Part A. 2006;77:426–35.

40. Pharr GM. An improved technique for determining hardness and elastic modulus using load and displacement sensing indentation experiments. J Mater Res. 1992;7:1564–83.

41. Farlay D, Armas LAG, Gineyts E, Akhter MP, Recker RR, Boivin G. Nonenzymatic Glycation and Degree of Mineralization Are Higher in Bone from Fractured Patients with Type 1 Diabetes Mellitus. J Bone Miner Res. 2016;31:190–5.

42. Polly BJ, Yuya PA, Akhter MP, Recker RR, Turner JA. Intrinsic material properties of trabecular bone by nanoindentation testing of biopsies taken from healthy women before and after menopause. Calcif Tissue Int. Springer; 2012;90:286–93.

43. Unal M, Uppuganti S, Leverant CJ, Creecy A, Granke M, Voziyan P, et al. Assessing glycation-mediated changes in human cortical bone with Raman spectroscopy. J Biophotonics. Wiley-VCH Verlag; 2018;11:e201700352.

44. Gamsjaeger S, Masic A, Roschger P, Kazanci M, Dunlop JWC, Klaushofer K, et al. Cortical bone composition and orientation as a function of animal and tissue age in mice by Raman spectroscopy. Bone. Elsevier; 2010;47:392–9.

45. Kazanci M, Fratzl P, Klaushofer K, Paschalis EP. Complementary information on in vitro conversion of amorphous (precursor) calcium phosphate to hydroxyapatite from raman microspectroscopy and wide-angle X-ray scattering. Calcif Tissue Int. Springer; 2006;79:354–9.

46. Awonusi A, Morris MD, Tecklenburg MMJ. Carbonate assignment and calibration in the Raman spectrum of apatite. Calcif Tissue Int. Springer; 2007;81:46–52.

47. Ellis R, Green E, Winlove CP. Structural analysis of glycosaminoglycans and proteoglycans by means of Raman microspectrometry. Connect Tissue Res. Taylor & Francis; 2009;50:29–36.

48. Gamsjaeger S, Robins SP, Tatakis DN, Klaushofer K, Paschalis EP. Identification of Pyridinoline Trivalent Collagen Cross-Links by Raman Microspectroscopy. Calcif Tissue Int. Springer New York LLC; 2017;100:565–74.

49. Nonlinear Optics - 3rd Edition. Available from: https://www.elsevier.com/books/nonlinear-optics/boyd/978-0-12-369470-6

50. Monnier VM, Kohn RR, Cerami A. Accelerated age-related browning of human collagen in diabetes mellitus. Proc Natl Acad Sci U S A. National Academy of Sciences; 1984;81:583–7.

51. Dudenkova V V., Shirmanova M V., Lukina MM, Feldshtein FI, Virkin A, Zagainova E V. Examination of Collagen Structure and State by the Second Harmonic Generation Microscopy. Biochem. Pleiades Publishing; 2019. p. 89–107.

52. Bank RA, Beekman B, Verzijl N, De Roos JADM, Nico Sakkee A, Tekoppele JM. Sensitive fluorimetric quantitation of pyridinium and pentosidine crosslinks in biological samples in a single high-performance liquid chromatographic run. J Chromatogr B Biomed Appl. Elsevier; 1997;703:37–44.

53. Bank RA, Jansen EJ, Beekman B, Te Koppele JM. Amino acid analysis by reverse-phase high-performance liquid chromatography: Improved derivatization and detection conditions with 9- fluorenylmethyl chloroformate. Anal Biochem. Academic Press Inc.; 1996;240:167–76.

54. Akin O, Göl K, Aktürk M, Erkaya S. Evaluation of bone turnover in postmenopausal patients with type 2 diabetes mellitus using biochemical markers and bone mineral density measurements. Gynecol Endocrinol. 2003;17:19–29.

55. Edward Hoffler C, Edward Guo X, Zysset PK, Goldstein SA. An application of nanoindentation technique to measure bone tissue lamellae properties. J Biomech Eng. J Biomech Eng; 2005;127:1046–53.

56. Rho JY, Zioupos P, Currey JD, Pharr GM. Variations in the individual thick lamellar properties within osteons by nanoindentation. Bone. Bone; 1999;25:295–300.

57. Lefèvre E, Farlay D, Bala Y, Subtil F, Wolfram U, Rizzo S, et al. Compositional and mechanical properties of growing cortical bone tissue: a study of the human fibula. Sci Rep. Nature Research; 2019;9:1–16.

58. Mulder L, Koolstra JH, Den Toonder JMJ, Van Eijden TMGJ. Intratrabecular distribution of tissue stiffness and mineralization in developing trabecular bone. 2007.

59. Nyman JS, Makowski AJ, Patil CA, Masui TP, O'Quinn EC, Bi X, et al. Measuring differences in compositional properties of bone tissue by confocal raman spectroscopy. Calcif Tissue Int. NIH Public Access; 2011;89:111–22.

60. Paschalis EP, Gamsjaeger S, Fratzl-Zelman N, Roschger P, Masic A, Brozek W, et al. Evidence for a Role for Nanoporosity and Pyridinoline Content in Human Mild Osteogenesis Imperfecta. J Bone Miner Res. John Wiley and Sons Inc.; 2016;31:1050–9.

61. Gamsjaeger S, Hofstetter B, Fratzl-Zelman N, Roschger P, Roschger A, Fratzl P, et al. Pediatric reference Raman data for material characteristics of iliac trabecular bone. 2014.

62. Currey JD. Role of collagen and other organics in the mechanical properties of bone. 2003.

63. Donnelly E, Chen DX, Boskey AL, Baker SP, Van Der Meulen MCH. Contribution of mineral to bone structural behavior and tissue mechanical properties. Calcif Tissue Int. NIH Public Access; 2010;87:450–60.

64. Taylor EA, Lloyd AA, Salazar-Lara C, Donnelly E. Raman and Fourier Transform Infrared (FT-IR) Mineral to Matrix Ratios Correlate with Physical Chemical Properties of Model Compounds and Native Bone Tissue. Appl Spectrosc. 2017;71:2404–10.

65. Boskey A. Bone mineral crystal size. Osteoporos. Int. Springer; 2003. p. 16–21.

APPENDIX A

PROTOCOL FOR NANOINDENTATION ON BONE

Protocol for Nanoindentation of Prepared Bone Samples

A. Supplies

1. Prepared sample of polished bone embedded in PMMA, glued to an AFM stub
2. Hysitron Nanoindenter

B. Starting Up

1. The nanoindenter is in Bard sub-basement, door password is 1498*

Figure 1: The 'box' under the nanoindenter. To zero the displayed load, use the AUTO ZERO function and the fine and course manual zero knobs.

2. The boxes under the nano-indenter are normally left on. If they are off, turn them on and wait for ~20 minutes to let the piezo equilibrate. Zero the bottom box either with auto zero or by turning the knob.
3. Turn on the software. If there are a bunch of crazy errors at this point, it probably means you need to zero.
4. Set the blue box behind the computer to QSM (quasistatic) mode.
5. Turn on the light box.

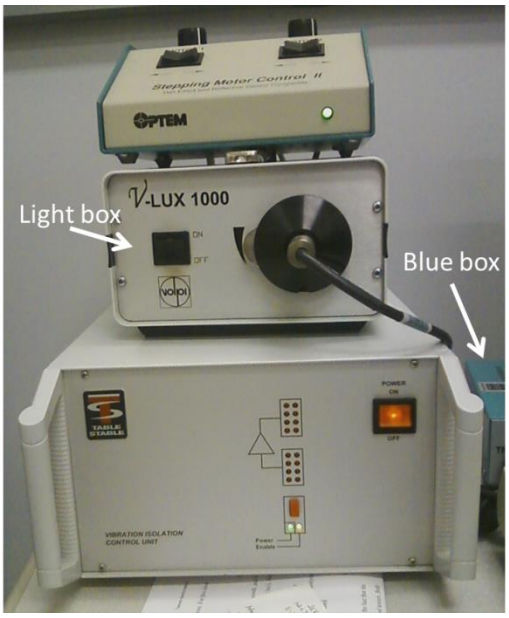

Figure 2: The light box and the 'blue box' are located to the left of the nanoindenter computer. Make sure the light is on, and the blue box is set to QSM.

C. Calibrating the Nanoindenter

1. Air Calibration
    a. Under the Calibration tab, check the transducer constants against the paper book.
    b. Set the low pass filter to 300, and the next two gains to 100 on the software. Set them that way on the physical box as well.

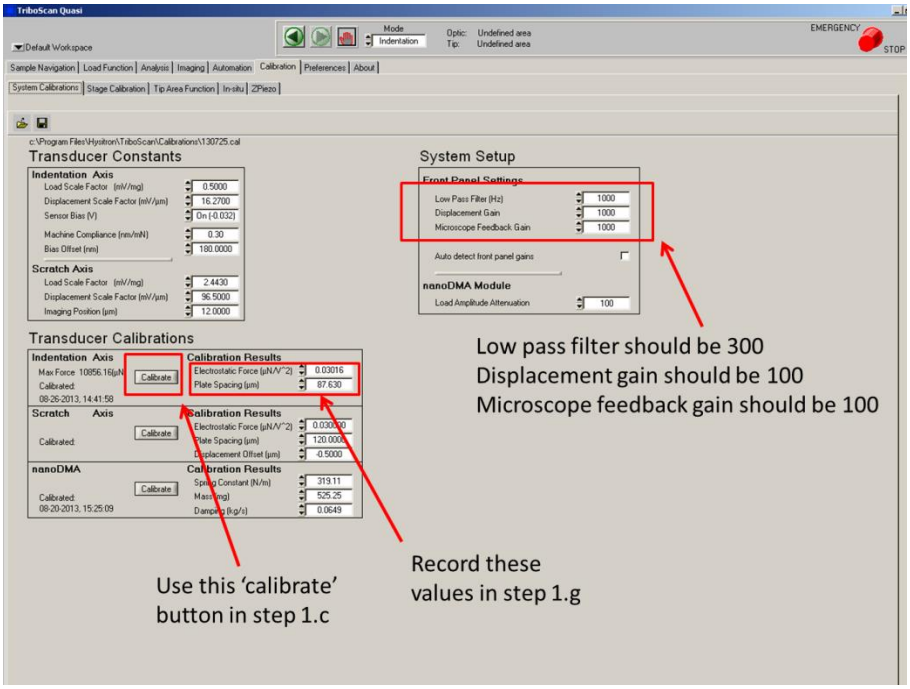

Figure 3: The 'calibration' tab of the triboscan software

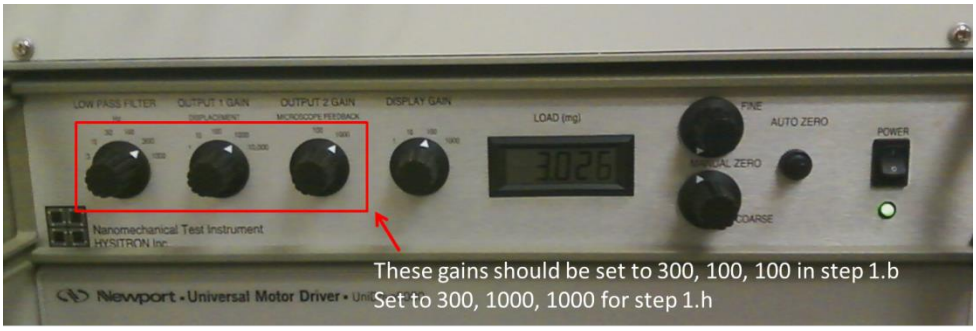

c. Press 'calibrate' button (the top one, there are several).

d. Set peak force to 1200 μN, rezero the box.

e. Press 'Cal air indent', and yes to keep this data.

f. After the calibration runs, close the curve fit and print screen a picture of the F vs. d cluster plot, and save this in your folder.

g. Record the electrostatic force and the plate spacing from the calibration tab in the notebook; they should be within 10% of previous calibrations.

h. Set the 2 second gains to 1000 on both the software and the box. Leave low pass at 300.

2. Quartz/Fused Silica Calibration

a. Under the sample navigation tab, find the edge of the quartz calibration sample. If the field of vision doesn't seem to be moving, you can disable the xy safety.

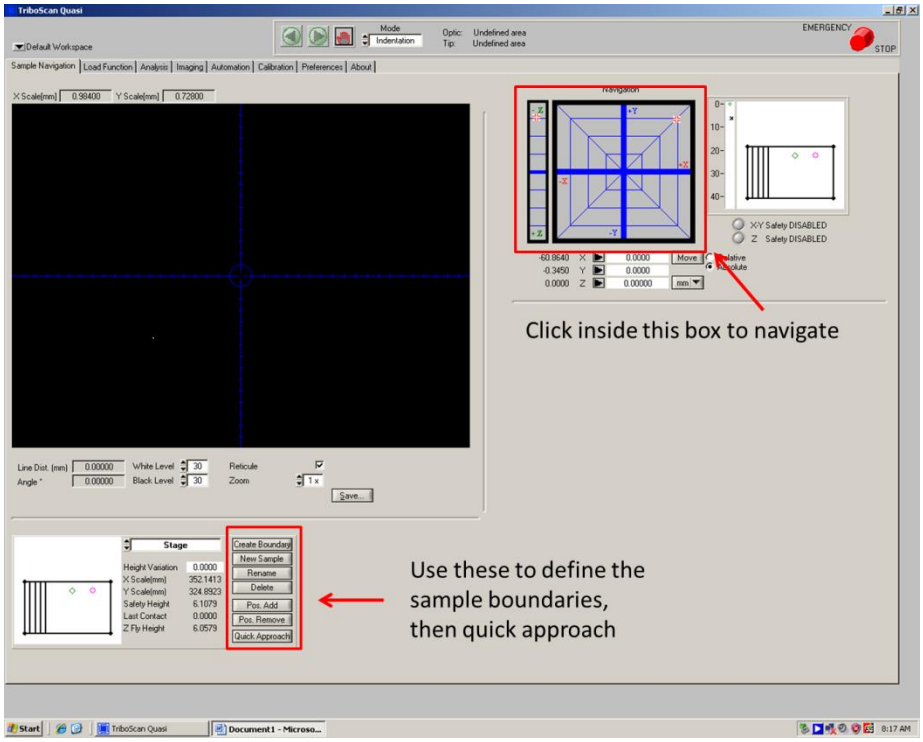

b. Focus on the edge of the quartz. The sample almost never moves, and should be at about 23mm in the z axis.

c. In the sample navigation tab, create and name a new sample.

d. Find the four corners of the quartz square, and at each point, 'add' the positions. You can refocus in z if necessary. It is better to be on the outside of the corners than inside.

e. Once the sample is defined, right click inside the small diagram of the sample shape to go to a position inside the sample.

f. Rezero the box, then press ‘quick approach’.

g. Go to the load function. File → Open load function → TRAPEZOID.ldf. Change the peak load to what you’ll be using (500 uN)

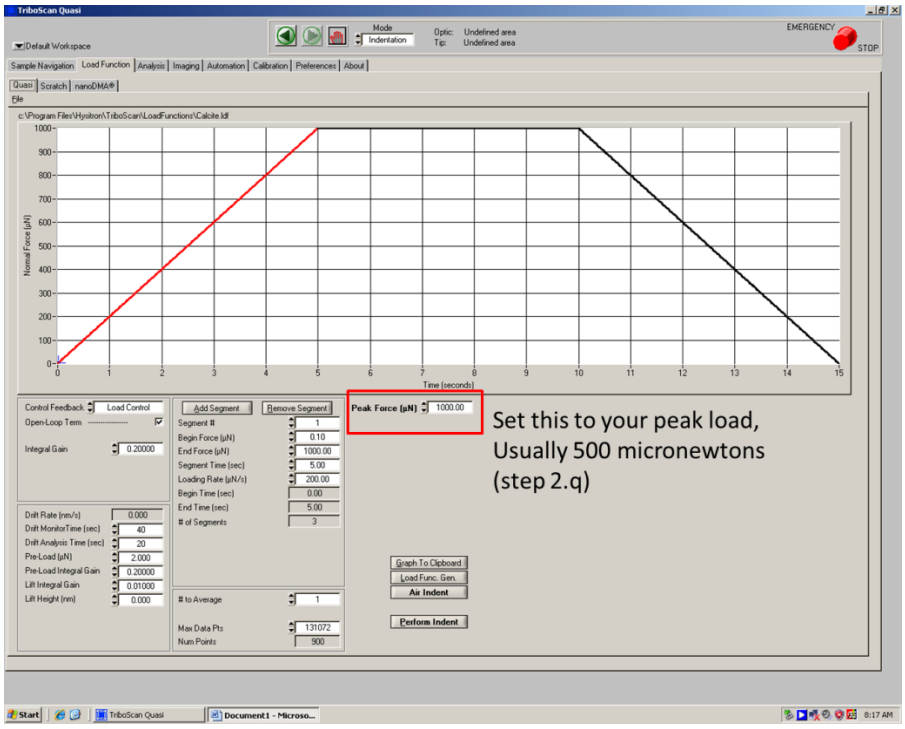

h. Click ‘run piezo automation’. On the popup, the start load and end load should be whatever you set in the previous step (both the same number, or else you don’t have a flat topped trapezoid.) This runs the quartz calibration.

3. Analyze the Quartz Calibration

a. Select unload segment 3.

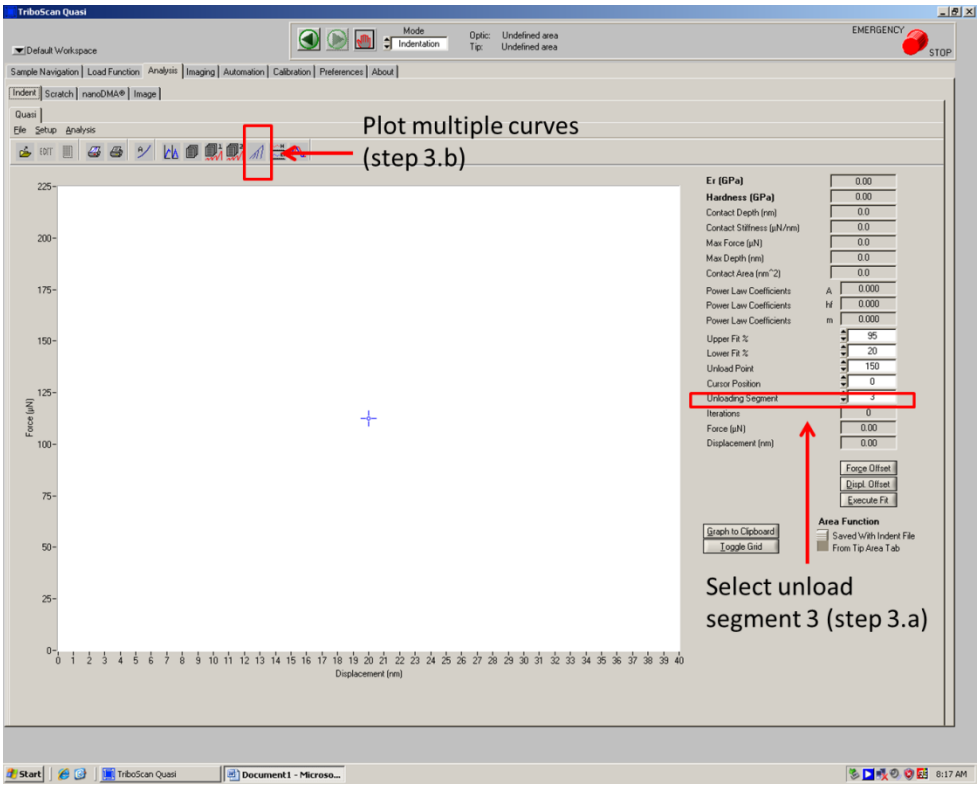

b. Select the 2nd blue squiggle, 'Plot Multiple Curves', for analysis.

c. Select and add all four calibration curves, then pick multi-curve analysis.

d. Record the mean values and std. deviations in the book. Make sure they're within 10% of the values gotten by people using the same max load.

e. When the scan is done, go to the imaging tab and unload.

D. Indenting on bone samples

1. Rehydrating the bone sample

   a. Rehydrate the bone tissue by immersing the tissue completely in Hank's Balanced Salt Solution (HBSS) for at least 2 hours. Longer times may be required for large samples.

b. Immediately perform nanoindentation after wiping the surface with a q-tip to remove any extra film of HBSS that may be lead to wrong surface detection and errors.

2. Setting up your sample
    a. Place your prepared sample of polished bone into the nanoindenter chamber. The base plate is magnetic, so the AFM stub should stick to it.
    b. Use steps ‘a’ through ‘e’ of the quartz calibration section above to define your sample area. Remember that it is better to include too much sample space than too little—the area defined now is the only space you will be able to indent in.
    c. Use the sample navigation tab to locate your area of interest on the bone, and position the reticule exactly over the location where you want the first indent to be.
    d. Optional: at this point, I like to take screenshots of the reticule on the exact 4 corners of my indent pattern, for future reference.
3. Creating and running a method automation
    a. Navigate to the ‘methods’ sub-tab of the ‘automation’ tab.

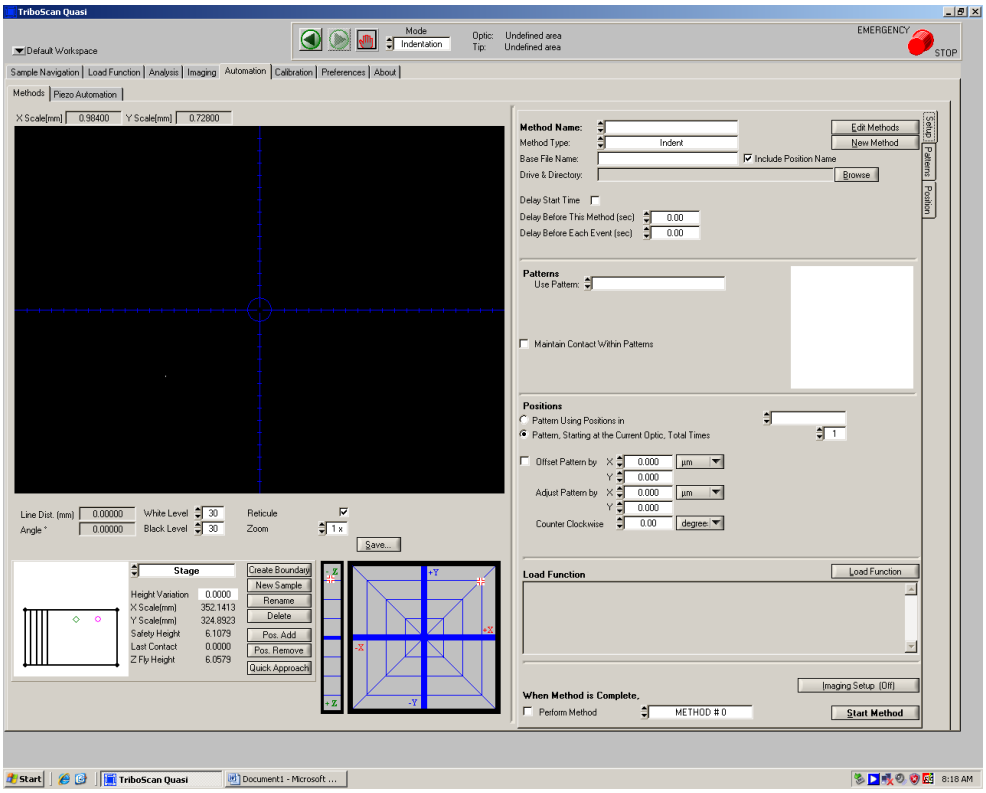

b. Select a name for your new method, as well as a base file name for the data and a drive and directory to save the data in.

c. Create a new pattern of whatever size and shape you want. A rectangular pattern with indents every 10-50 microns is a good start. Make sure that you keep in mind whether your area of interest is oriented landscape-wise or portrait-wise, and that your pattern is set to start on whichever corner you placed the reticule at.

d. Save this new pattern, then select it under the methods tab. Do not maintain contact within the pattern.

e. If you need to rotate the view to correctly indent your area of interest, do this under the ‘Positions’ heading.

f. Set up your load function. This should be the same load function that you used for quartz calibration.

g. Once all the method parameters are set up to your satisfaction, press ‘Start Method’. A note to keep in mind—each indent takes about 4 minutes, so large methods will take a long time to run.

4. Analyzing the data

   a. Follow steps ‘a’ through ‘c’ of analyzing the quartz calibration to get hardness and reduced modulus values for each sample indent. Be sure to record which positions go with which indent numbers using the diagram at the bottom right hand corner of the screen.

APPENDIX B

PROTOCOL FOR CONFOCAL AGE AND COLLAGEN MAPPING OF BONE

Supplies

1. Planar parallel bone sample
    a. roughness ~ at least microtome cut roughness
2. HBSS (depending on objective)
3. Petri dish, deep (for dipping lens, ex. 20X, 1.0 NA)
4. Microscope slide
5. Coverslip

Instrument startup

1. If the computer is off, turn it on and let it boot.

2. Check that objective turret position is set to the objective you need. If the objective you need is not equipped in the turret, follow the steps in next section to change the objective.

3. Turn on the main switch.

4. Turn on the Systems/PC switch. Wait until touchscreen boots.

5. Turn on the Components switch.

6. Log in to the computer. (Username – *netID@cornell,edu*; Password – *netID password*)

7. Check manual slider. It must be empty for standard confocal detection.

8. Start “Zen” software and click on the “Start System” button.

9. Turn on lasers you will be using (405 nm and MaiTai (780 nm)). The Ar and multiphoton lines (MaiTai) take ~5 min to turn on. You can follow the warm-up progress by selecting the laser you are using and the Laser Properties (located below laser list).

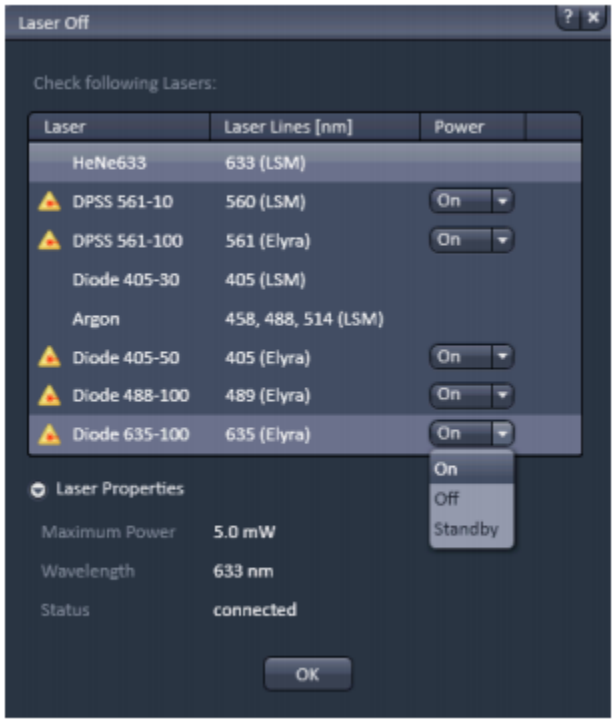

Changing objectives

1. Move nosepiece to an empty position or unscrew one of the current objectives (if all positions are full). Make sure you put the objective taken out in the objective cabinet.

2. Screw in your desired objective. Do not let the objective drop!! **Please handle the objective with care**.

3. In Zen, go to the Maintain tab.

4. Click on Objectives tab.

5. Check the nosepiece position of your objective, then under Detection Objective, click on the objective icon in that particular position.

6. Under Change Objective, click on Favorite Objectives. You will see a list of objectives.

7. Choose your objective (name, magnification, NA, immersion), then on the menu on the left, click on Select Objective. There are several listings that are similar, ask Johanna if you are not sure which objective to select.

8. Click Write to Hardware.

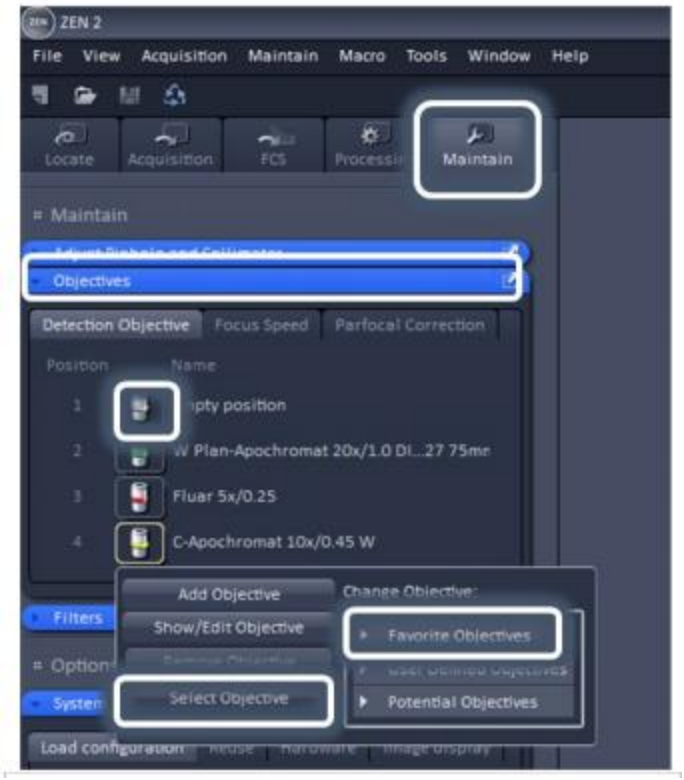

9. When you go back to the Locate tab, your objective name should be displayed correctly.

Setting up the sample

For dipping lens (20X, NA 1.0)

1. Place your sample in a petri dish and submerge it with HBSS. Make sure there is enough working space in X,Y and Z directions. The working distance of the dipping lens is 2.4 mm.

2. Move the stage using the joystick so that the sample is approximately under the objective. Make sure the HBSS is not spilt when moving the stage.

3. Use the coarse adjustment knob to move the objective in Z-direction and dip the objective in HBSS.

4. Click on the Locate tab, looking through eyepiece, find the focus using the coarse and fine adjustment knobs. Take extreme care not to crash the objective into the sample.

AGE mapping

1. Switch to 405 nm laser and use LSM mode and set the spectral collection to 430 nm - 450 nm. Set the pinhole aperture to collect fluorescence from 1 um thick optical section.

2. Click on the Live button. You will see a faint blue laser line being incident on the sample.

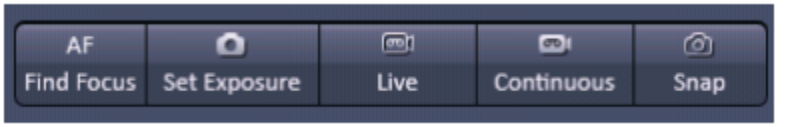

3. Check the computer screen for fluorescence signal on the screen and using the fine adjustment knob, adjust the focus while ensuring appropriate distance between objective and the sample.

4. Adjust the gains and power (usually 5% but max. 10%) until you are satisfied with the quality of the image. Disadvantages of high gains…

5. Click on Snap to collect the image and right click on the image in the file handling area and save it in your folder.

6. The endogenous AGEs photobleach very quickly. So, be quick and turn off the Live when you are not imaging.

SHG mapping

1. Replace the slider with the NDD slider. Note the arrows and never force the slider into the slot.

2. Adjust the dials on the Berek Waveplate to circularly polarize the light. (for 780 nm, LCP – 158/10)

3. Turn-off all the lights in the room. Cover the entire microscope setup with a black cloth to block light from the monitor entering the detectors.

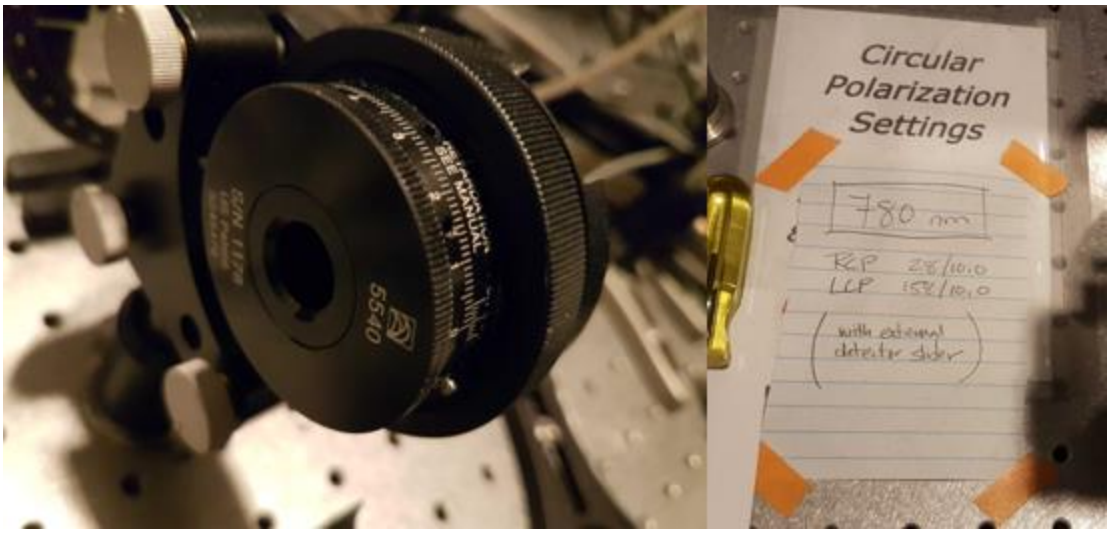

4. Change the laser line to MaiTai and enter 780 nm for the wavelength. Wait if the laser icon turns red. Click on NDD mode. NEVER use the NDD mode with the lights turned on.

5. Click Live and while looking at the screen adjust the focus. Adjust the gains and power (usually 5% but max. 10%) until you are satisfied with the quality of the image.

6. Click on Snap to collect an image and save it.

6. Switch off the detection line and then turn on the lights.

APPENDIX B

PROTOCOL FOR ATOMIC FORCE MICROSCOPY ON BONE

Materials: Polished sample embedded in PMMA and mounted on AFM stub (for more information see precision polishing protocol) and AFM tips (purchased from CCMR – Email Steve Kriske (sjk27@cornell.edu) to purchase cantilevers)

Purpose: To measures the surface roughness of a sample prior to performing Raman and nanoindentation in order to establish the appropriate measurement settings.

Methods:

1. Fill out the Asylum MFP-3D AFM usage sheet found in the binder next to the computer monitors for the instruments.
    a. AC mode used, standard mode used, CCMR supplies cantilever
2. Enable the AFM in Coral (or FOM) to use the left monitor that is interlocked to Coral enabling.
3. Load the cantilever into the 3D standard cantilever holder (Figure 1)
    a. Carefully remove supplied cantilever from the box with tweezers (if cantilever falls on table/ hard surface, the tip may break or deform and you may need to use a new cantilever – check if the tip is intact or broken by viewing the cantilever under bright light)
    b. Slide the cantilever probe under the clip on the cantilever holder with tweezers. A good estimate for how far to push is - the etched line on the cantilever should be

just visible after inserting the cantilever into the clip. Make sure the cantilever is orthogonal to the holder and pointed away from the holder

c. Screw in cantilever to cantilever holder. Do not overtighten the clip to the point of bending the cantilever.

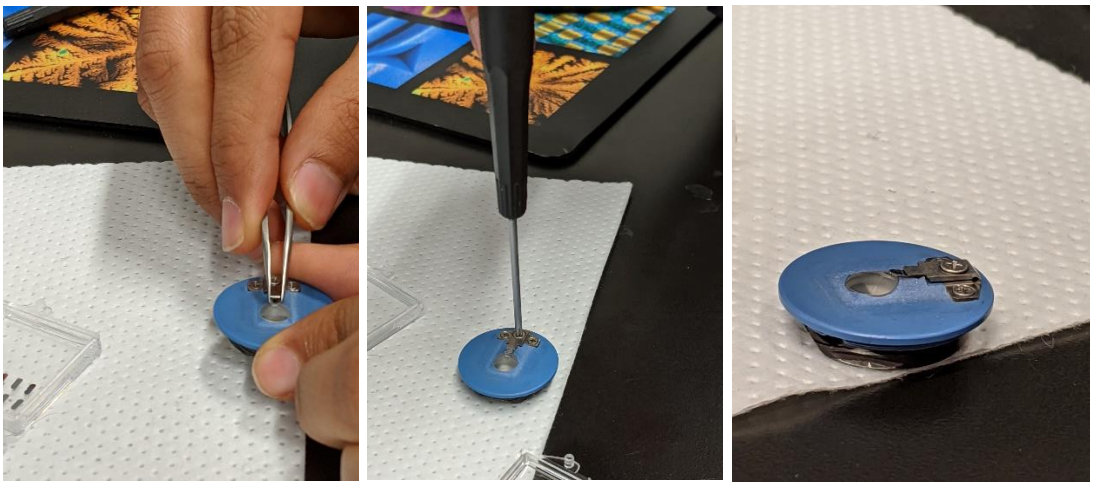

Figure 1. Inserting cantilever to cantilever holder with tweezers, screwing the cantilever into the cantilever holder, and resulting mounted cantilever in cantilever holder

4. Place sample on AFM stage
    a. Install the magnetic sample holder to the stage
    b. Place a sample glued to AFM stub on the sample holder
    c. Secure the holder in place with magnets.

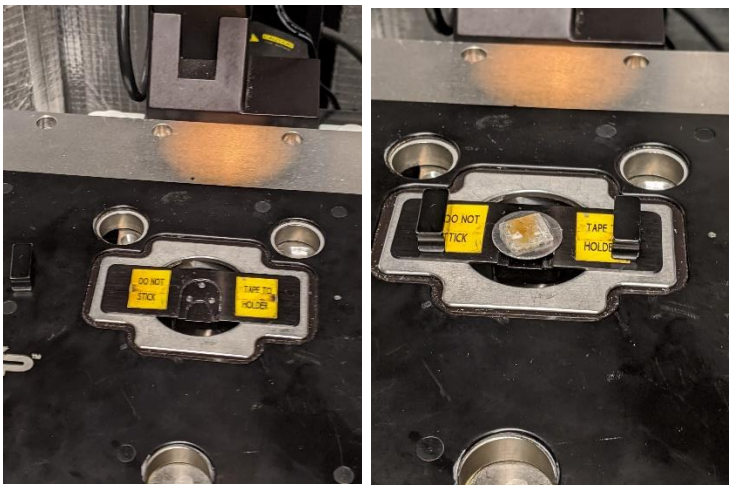

Figure 2. Adding magnetic sample holder to state and placing sample (glued to AFM stub) to magnetic sample holder and securing with magnets.

5. Insert the cantilever holder on the AFM head by pressing the button on the right side of the cone and release the button (Figure 3).

Figure 3. Cantilever holder added to AFM head

6. Before placing the AFM head on the stage, make sure to lift the legs according to sample thickness using the thumbwheel and then place the head on the stage carefully in the appropriate holes in the sample stage.

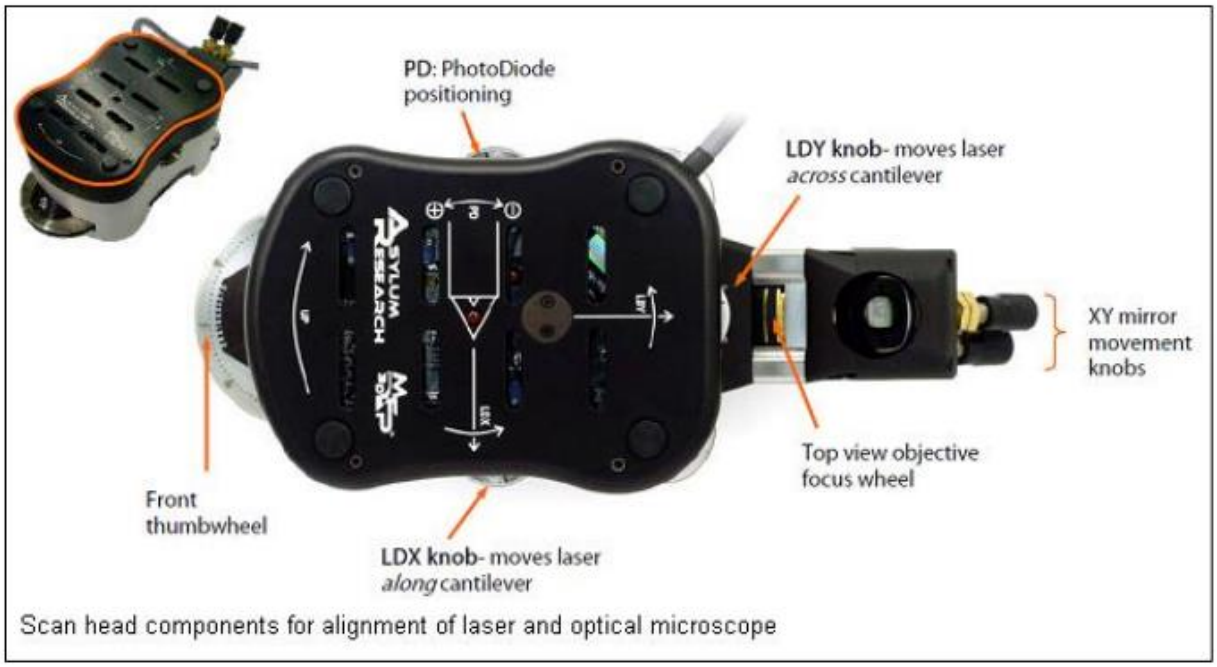

Figure 4. Scan head components

7. Open the Asylum Research V13 software on the computer. In the Mode Master, select Standard>Topography>AC air topography or open a desired experiment file.
8. Click the camera icon in the bottom of the software to initialize the video window.
9. Turn on illumination and control the intensity according to image in the video window.
10. Find the cantilevering the video by moving the field of view using the XY mirror movement knobs. Adjust the focus wheel in order to focus the cantilever.
11. Turn the laser on by turning the key switch on the ARC2 controller.
12. Focus the laser on the cantilever tip using LDX and LDY dials
13. Maximize the 'Sum' (in Sum and Deflection Meter Window) without losing focus on the far end of the cantilever by moving LDX and LDY dials (sum of 4.5-5 is sufficient)

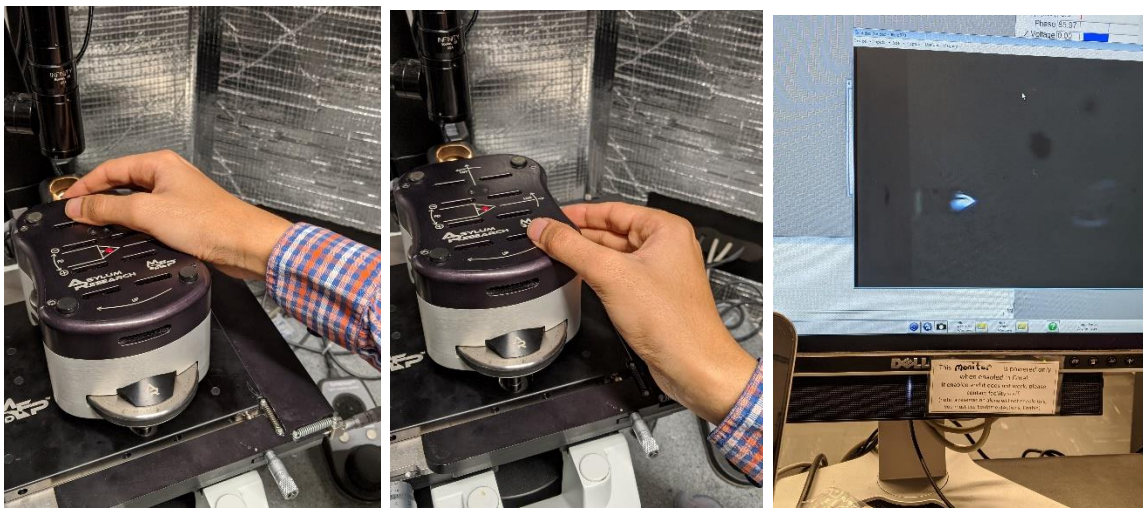

Figure 5. LDX and LDY adjustment dials used to adjust laser position and laser properly focused on an AFM tip

14. Set the deflection to 0 (+/- 0.05) with PD dial

Figure 6. Adjusting the PD dial on the side of the AFM head

15. Approach cantilever to sample using the front thumbwheel (note you will need to adjust the field of view using the XY mirror knobs to keep the cantilever tip in the field of view) until approximately 1mm from the sample (seen visually)

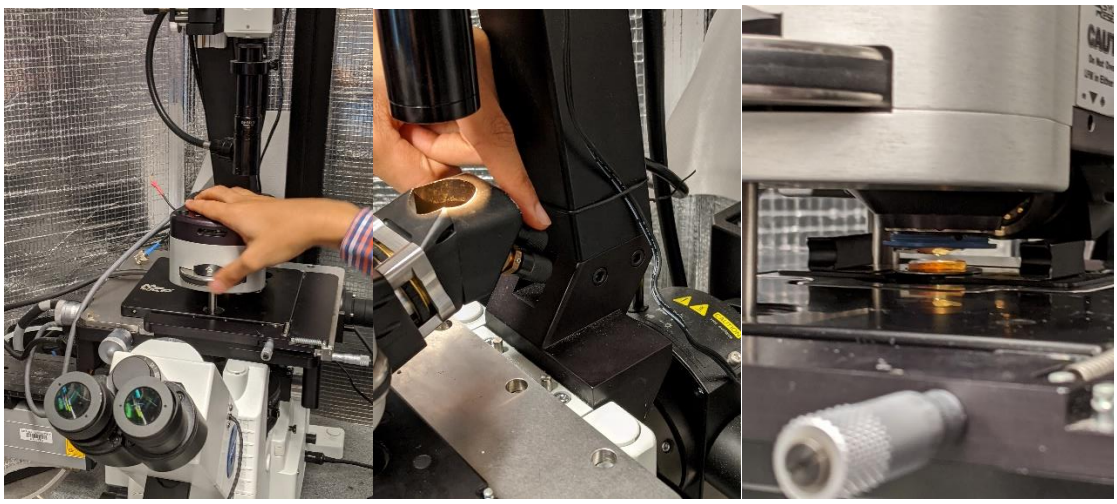

Figure 7. Lowering the AFM head while maintaining focus on the sample until head is approximately 1mm from the sample

16. Tune cantilever
    a. In the Master Panel, open the Tune tab and under Auto Tune, select target amplitude of 1V and target percentage of +5% (non-contact mode) or -5% (tapping mode)
    b. Click autotune. After a few seconds, a tone can be heard, and a graph will be displayed which can be minimized or closed.
17. Engage Piezo by clicking engage in sum and deflection meter window
    a. Z voltage should go to 150 (if z voltage is -10 when engaged you forgot to tune the cantilever)
18. Continue to approach the sample using the front thumbwheel and XY mirror knobs to keep the cantilever in the field of view
    a. Sample should come into focus in the video when the cantilever is close to the sample

b. Use the X and Y micrometer knobs on the stage to find a region of interest on your sample. You can use the microscope focus wheel to bring the focus down to the sample and then find the region of interest on your sample. Make sure to change focus back to the cantilever after finding the region of interest.
c. Once you are satisfied with the region of interest, move the head down with the front thumbwheel. If the cantilever is in contact with the sample, the amplitude will go to 0.8 and a tone can be heard

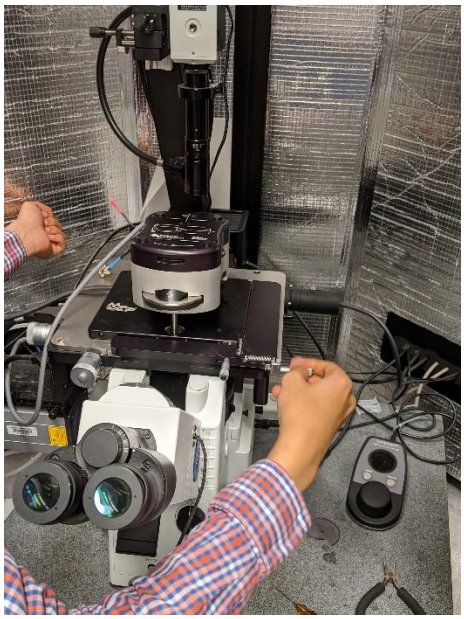

Figure 8. Moving the stage to focus on a region of interest in your sample

19. Lower AFM head until z voltage goes to ~70
20. Begin scan (master panel window, main subheading)
    a. Scan size usually 5x5 microns
    b. Scan rate initially at 1Hz (default)
    c. Set point 800mV (default)

d. Integral gain 10 (default)

e. To save images separately click ‘setup’

   i. Provide a base file name for sample (file name must include characters)

   ii. Set file path to Asylum research data user folder

f. Click ‘do scan’ to begin scanning

21. Optimize Height retrace graph/ collect scan

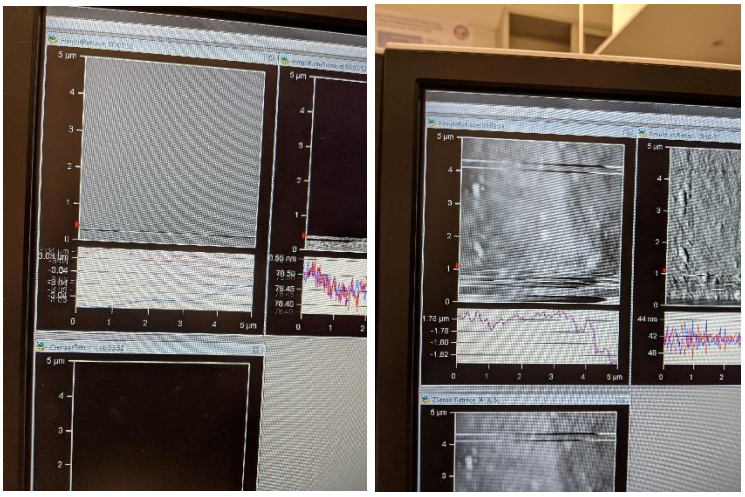

Figure 9. Height retrace window displaying out of phase and in phase blue and red lines

a. Red and blue lines should be on top of each other. If they are not, lower the set point in the master panel until they match approximately, and a good image is forming in the Height Retrace window.

   i. If you reduce the set point, the Z-voltage will increase. If the Z-voltage reaches 150, you will have to lower AFM head using the front thumbwheel until Z-voltage returns to 70

   ii. Do not go below a set point of 500, it damages the tip. However, if your tip is damaged or old, you may have to go below a set point of 500

   iii. For a new tip, the set point is around 600

b. If the red and blue lines still do not match after you have lowered the set point,
    i. Reduce the ‘scan rate’ (Eg. 0.8Hz or 0.5Hz)
    ii. Consider increasing the ‘integral gain’ (Eg. 14.77)
    iii. Restart the scan (Click ‘frame up’/’frame down’)
c. If you cannot get the red and blue lines to align even after all the above changes, your tip may be damaged, consider trying a new tip.

22. Once a full 5x5 um scan is completed, click on ‘stop scan’ (piezo retracts automatically)
    a. Z voltage should go to 0
23. Analyze scan
    a. Click AFM analysis>Browse Saved Data. Double click the image you want to analyze.
    b. Go to AFM analysis>Analyze panel to get the RMS roughness.
    c. If the image contains blurry regions, try to scan again. Or, Click M in height retrace window to generate a mask and exclude those regions.
    d. Record the RMS values of roughness.
24. Raise AFM head slightly until amplitude becomes ~1 (cantilever no longer toughing sample)
    a. Note you will have to refocus on the sample using microscope dial
    b. If you accidentally move the laser, you will have to re-tune it
25. Use the micrometer knobs on the stage to find a new region of interest on the sample
    a. Repeat steps 17-24 to scan again (scan at least 3 regions per bone tissue compartment to characterize the sample completely)
26. When scans are completed

a. Stop scan by clicking ‘stop!!!’ or ‘stop scan’
b. Raise AFM head significantly above the sample using the front thumbwheel
c. Remove AFM head and place it upside down on holder next to AFM
d. Remove the AFM cantilever holder from the AFM head
e. Remove the cantilever from AFM cantilever holder with tweezers
    i. Return the cantilever to the cantilever storage box
    ii. Return the cantilever holder to the cantilever holder box
f. Remove the sample and the magnetic holder from the stage. Close and latch the doors of the instrument.
g. Save the workspace in your folder on the computer and close the program
h. Turn off the left screen by clicking ‘disable’ after selecting Asylum AFM in Coral.
i. Sign out in Asylum log sheet